

# Petrogenesis and Tectonic Implications of the Yuhuashan A-Type Volcanic-Intrusive Complex and Mafic Microgranular Enclaves in the Gan-Hang Volcanic Belt, Southeast China

Kui-Dong Zhao,\* Guo-Qi Liu, and Shao-Yong Jiang

State Key Laboratory for Geological Processes and Mineral Resources and Collaborative Innovation Center for Scarce and Strategic Mineral Resources, Faculty of Earth Resources, China University of Geosciences, Wuhan 430074, People's Republic of China

## ABSTRACT

Early Cretaceous felsic volcanic-intrusive complexes are widespread in the Gan-Hang Volcanic Belt (GHVB) and accompany abundant uranium ore resources. However, the petrogenesis and tectonic significance of these rocks are not well understood. We present zircon U-Pb geochronology, major- and trace-element geochemistry, and Sr-Nd-Hf isotopic compositions of the Yuhuashan Complex and hosted mafic microgranular enclaves (MMEs) from the south-western part of the GHVB. The Yuhuashan Complex consists of rhyolitic porphyritic lava and subvolcanic porphyritic granite that are metaluminous to weakly peraluminous and have pronounced A-type geochemical characteristics. They were formed at a high temperature and can be further classified as  $A_2$  subtype affinity. The Yuhuashan A-type granitic rocks were generated largely by partial melting of Proterozoic metamorphic rocks. Our new data, together with previously published data, suggest that the Early Cretaceous  $A_2$ -type granitic rocks formed along the GHVB during an extensional event. The MMEs hosted in the Yuhuashan porphyritic granite exhibit igneous textures, suggesting quenching of mafic magmas that comingled with the host granitic magma. Zircons from the MMEs have similar U-Pb ages but higher  $\varepsilon_{\text{Hf}}(t)$  values, compared to the host granite. Hence, the MMEs and host granite likely crystallized from different magma sources, providing direct evidence for mafic-felsic magma-mingling processes. The MMEs have high MgO and  $K_2O$  contents and show shoshonitic affinities. Geochemical and isotopic data imply that the MMEs were derived from a phlogopite-bearing lithospheric mantle source that had been metasomatized by previous subduction-related fluids or melt. Underplating of such high-temperature mafic magmas could have induced lower-crustal rocks to partially melt and generate the Yuhuashan A-type complex. A backarc extensional setting, related to the rollback of a subducted paleo-Pacific-derived plate, is favored to explain the petrogenesis of the Yuhuashan Complex and MMEs.

**Online enhancements:** supplemental tables.

## Introduction

Extensive felsic magmatic activity occurred in Southeast China during the late Mesozoic, forming an approximately 600-km-wide igneous zone (fig. 1) that has been suggested to represent one large felsic igneous province (Wang and Zhou 2005). The origin and evolution of the late Mesozoic magmatic zone are thought to be due to subduction of a paleo-Pacific-derived plate beneath the

Eurasian plate (e.g., Charvet et al. 1994; Lapierre et al. 1997; Zhou and Li 2000; Li et al. 2014). But different subduction processes of the paleo-Pacific plate have been suggested, including a successive-subduction model (Jahn et al. 1990; Li et al. 2014), a shallow-subduction-and-rollback model (Zhou and Li 2000; Liu et al. 2014), the foundering of the flat-subducting plate (Li and Li 2007), and subduction with changing directions (Sun et al. 2007). Establishing the processes and controls on the generation of the magmatic zone remains a major challenge relevant to the tectonic evolution of the South China Block (SCB).

Manuscript received February 27, 2018; accepted August 6, 2018; electronically published December 7, 2018.

\* Author for correspondence; email: zhaokd@cug.edu.cn.

[The Journal of Geology, 2019 volume 127, p. 000–000] © 2018 by The University of Chicago.  
All rights reserved. 0022-1376/2019/12701-0003\$15.00. DOI: 10.1086/700408

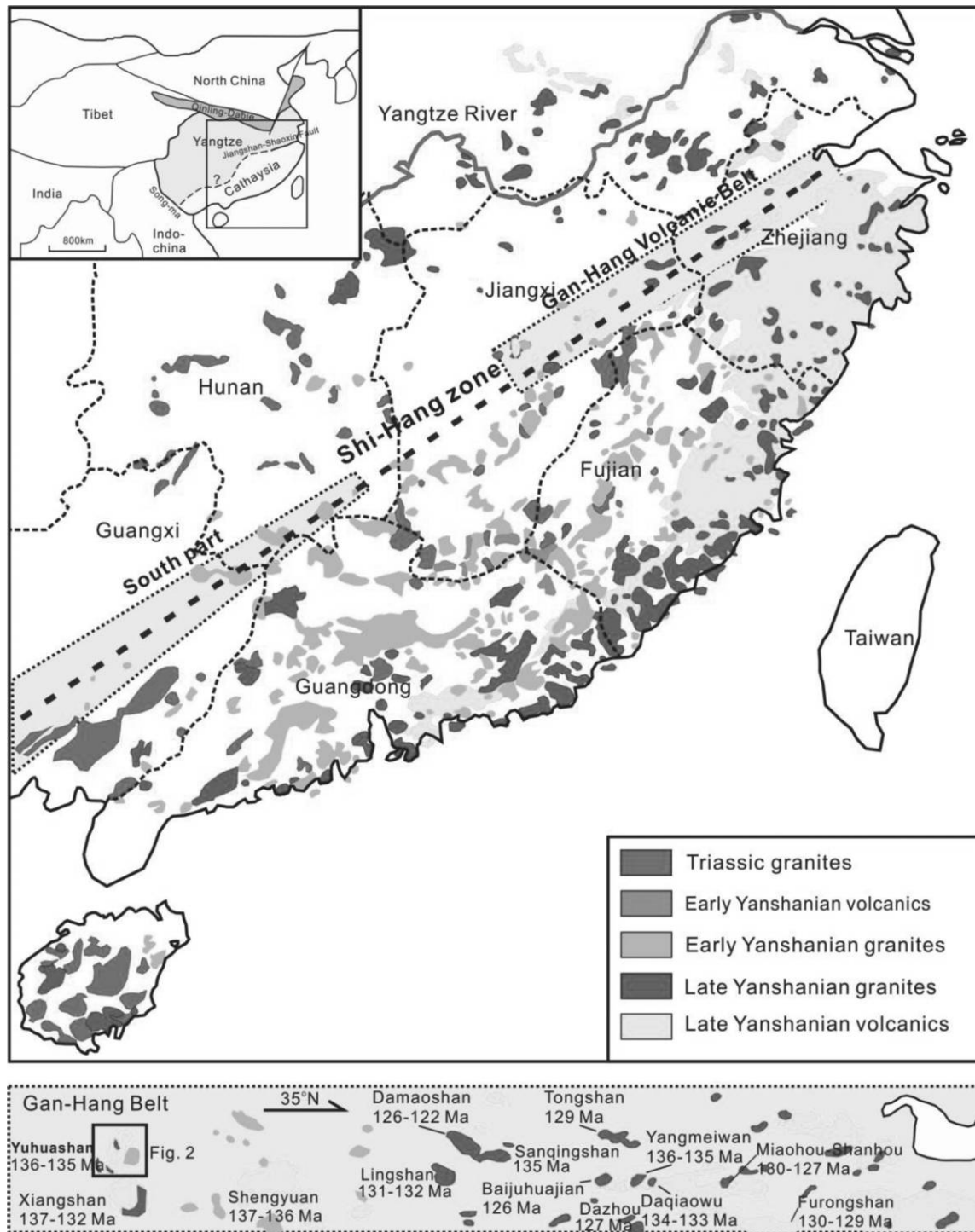


**Figure 1.** Distribution of Mesozoic granites and volcanic rocks in Southeast China and major Early Cretaceous volcanic and intrusive rocks in the Gan-Hang Belt. A color version of this figure is available online.

The “Shi-Hang zone” (SHZ) was first proposed by Gilder et al. (1991) for a NE-trending belt that runs from the Shiwan Mountains to Hangzhou City in the interior of the SCB (fig. 1). The SHZ contains many igneous rocks with high  $\varepsilon_{\text{Nd}}(t)$  values (above

–8) and young  $T_{\text{DM}^c}$  model ages (<1.6 Ga; Gilder et al. 1996). The zone also contains many economically important mineral deposits and is regarded as a metallogenic belt (also called the Qin-Hang Mineralization Belt; Mao et al. 2011). The SHZ has been

subdivided into southern and northern parts (Chen and Jahn 1998), with the northern part coinciding with the Gan-Hang Volcanic Belt (GHVB), which contains a series of volcanic basins and volcanic-intrusive complexes (fig. 1). The SHZ was initially interpreted as the result of mantle upwelling along a paleorift (Gilder et al. 1991). Many granitic rocks in the SHZ have now been identified as A-type; thus, a lithospheric extensional setting is now generally favored for the formation of the SHZ (e.g., Jiang et al. 2005; Wong et al. 2009; Zhao et al. 2012; Shu et al. 2017). The relatively high  $\varepsilon_{\text{Nd}}(t)$  values of these igneous rocks, compared to typical continental crust in South China, have been interpreted to be caused by involvement of juvenile, mantle-derived magma (e.g., Gilder et al. 1996; Zhao et al. 2010, 2012; Wang et al. 2015). However, synchronous mafic rocks are rare in this region, and the existence of a tectonic regime of asthenosphere upwelling is speculative (e.g., Jiang et al. 2011; Xia et al. 2016).

The Yuhuashan felsic volcanic-intrusive complex lies in the southernmost part of the GHVB (fig. 1) and contains abundant mafic microgranular enclaves (MMEs) hosted in the subvolcanic porphyritic granite. The primary magma for MMEs has generally been suggested to be derived from mantle sources; hence, MMEs can provide valuable information about the deep magmatic dynamics (e.g., Didier and Barbarin 1991; Yang et al. 2007; Zhao et al. 2012). In this article, we present a detailed investigation on the petrography, zircon U-Pb ages, major- and trace-element geochemistry, and Sr-Nd-Hf isotope data for both the Yuhuashan Complex and the MMEs, with the objective of identifying the origin of the crust- and mantle-derived magma and thus gaining better understanding of the geodynamic setting responsible for formation of the GHVB.

### Geological Setting

The SCB is bordered by the North China Craton to the north, the Tibetan Plateau to the west, the Indochina Block to the southwest, and the Philippine Sea plate to the east. The SCB is composed of the Yangtze Block and the Cathaysia Block, on the basis of their distinctive crustal ages and tectonic evolution histories (e.g., Qiu et al. 2000; Xu et al. 2007). The boundary between the Yangtze Block and the Cathaysia Block is the NE-trending Jiangshan-Shaoxing Fault, but the southwestern extension of this boundary is ambiguous because of poor exposure and multiple intensive tectonic modifications. The amalgamation of the Yangtze Block

and the Cathaysia Block likely occurred in the Neoproterozoic (e.g., Li et al. 2009; Charvet 2013). The united SCB underwent at least three tectonic-magmatism events during the Late Ordovician–Silurian, Triassic, and Jurassic–Early Cretaceous deformation phases.

During the Jurassic–Cretaceous, the SCB hosted widespread and intensive magmatism in the form of many volcanic-intrusive complexes (fig. 1). The associated granitic rocks appear to be younger toward the coast, with the Jurassic ages found inland and Cretaceous ages along the coast (e.g., Zhou et al. 2006). The Cretaceous volcanic rocks mainly crop out along the coast, with minor occurrences inland along the GHVB (fig. 1).

The GHVB is superimposed on the Jiangshan-Shaoxing Fault, and it extends at least 450 km in a NE-SW direction. A series of Jurassic–Early Cretaceous volcanic basins and granitic complexes occur within the GHVB (fig. 1). Late Cretaceous extensional red-bed basins formed concurrently with the latest phase of the regional magmatism and were infilled with volcanic rocks, red clastic sedimentary rocks, marl, gypsum, and evaporates. The sediments have a total thickness of more than 10 km.

Early Cretaceous felsic volcanic and intrusive rocks are widespread in the GHVB (fig. 1), but coeval mafic rocks are rare (e.g., Jiang et al. 2011; Xia et al. 2016). The results of recent detailed investigations of the geochronology and geochemistry of these complexes are summarized in table 1. Since the late 1950s, a number of large-scale uranium deposits have been explored and mined in the GHVB. These deposits mainly occur in the Early Cretaceous volcanic complexes, in which the Xiangshan Complex hosts the largest volcanic rock-hosted uranium deposit in China. The Yuhuashan Complex lies to the northwest of the Xiangshan Complex, and the two are separated and overlain by Cretaceous red beds within a NNE-trending basin.

The outcropping basement rocks in the study area belong to the Proterozoic metamorphic rocks (the Zhoutan Group) and consist of schists, granulites, and amphibolites. The protoliths of the schists and granulites were suggested to be of sedimentary origin, whereas the precursor of the amphibolites was of basaltic origin (Hu and Zhang 1998).

The Yuhuashan Complex comprises a collapsed caldera and resurgent dome association. The Yuhuashan caldera is approximately 32 km long and 15 km wide, covering an area of about 330 km<sup>2</sup> (fig. 2). The volcanic-intrusive rocks mainly comprise rhyolitic porphyritic lava and associated subvolcanic porphyritic granite. The porphyritic gran-

**Table 1.** Review of the Major Early Cretaceous Volcanic and Intrusive Rocks along the Gan-Hang Volcanic Belt

Name	Rock type	Age (Ma)	$\epsilon_{\text{Nd}}(t)$	Type	References
Yuhuashan	Porphyritic lava	136	-8.1 to -7.6	A-type	This study
Yuhuashan	Porphyritic granite	135	-8.1 to -7.4	A-type	This study
Yuhuashan	Mafic enclaves	135	-7.2 to -5.2		This study
Xiangshan	Rhyodacite, lava	132-136	-8.3 to -7.4	A-type	Yang et al. 2011
Xiangshan	Granite porphyry	136-137	-8.7 to -6.9	A-type	Yang et al. 2011
Xiangshan	Mafic enclaves		-7.2 to -4.2		Jiang et al. 2005
Shengyuan	Tuff	136-137	-12 to -9	A-type	Shu et al. 2017
Lingshan	Alkali-feldspar granite	131-132	-4.1 to -2.7	A-type	Zhou et al. 2013
Damaoshan	Alkali-feldspar granite, syenogranite	122-126	-5.4 to -1.4	A-type	Jiang et al. 2011
Sanqingshan	Alkali-feldspar granite	135	-3.3 to -1.0	A-type	Zhou et al. 2013
Bajuhuaian	Alkali-feldspar granite	126	-2.55	A-type	Wong et al. 2009
Dazhou	Rhyolite	127	-6.4 to -5.5	A-type	Yang et al. 2013
Tongshan	Alkali-feldspar granite, syenogranite	128-129	-5.6 to -2.2	A-type	Jiang et al. 2011
Tongshan	Diabasic dike	129	+0.9		Jiang et al. 2011
Ehu	Two-mica granite	122-124	-7.4 to -7.1	S-type	Jiang et al. 2011
Yangmeiwan	Granite	135-136	-6.5 to -3.6	A-type	Yang et al. 2012
Daqiaowu	Granitic porphyry	133-134	-5.8 to -5.0	A-type	Yang et al. 2012
Miaohou	Granitic porphyry	127-129	-4.6 to -2.3	A-type	Xia et al. 2016
Miaohou	Diabase dike	127-130	-2.3 to -2.1		Xia et al. 2016
Shanhou	Granitic porphyry	128	-3.5		Xia et al. 2016
Shanhou	Diabase dike		+1.7		Xia et al. 2016
Furongshan	Alkaline feldspar granite	129-130	-3.7 to -3.3	A-type	Wang et al. 2015
Furongshan	Mafic enclaves	127	-3.2 to -2.9		Wang et al. 2015

ite mainly occurs in the central part of the caldera and along the ring fractures (fig. 2). The Triassic Maixie granite lies to the west of the Yuhuashan Complex and was intruded by the porphyritic granite. The Jurassic Ziyunshan granite pluton lies to the east of the Yuhuashan Complex.

### Petrography

The rhyolitic porphyritic lava is the main volcanic rock type in the Yuhuashan Complex. It is generally gray in color and has a fragmental texture (fig. 3a, 3b), consisting of crystal phenocrysts (0.1–0.2 mm, ~50 vol%), glass fragments (0.05–0.1 mm, ~10 vol%), fine-grained volcanic ash (<0.05 mm, ~20 vol%), and lithic fragments such as schist (~20 vol%). The main crystal minerals include quartz (~20 vol%), alkaline feldspar (~20 vol%), plagioclase (~5 vol%), biotite (~5 vol%), and minor accessory minerals such as apatite, zircon, and allanite.

The subvolcanic porphyritic granite is light gray, with a porphyritic texture (fig. 3c). The phenocrysts (~30 vol%) are mainly K-feldspar and plagioclase, up to 3–4 cm in length. The groundmass has a medium-grained granitic texture consisting mainly of alkaline feldspar (~35 vol%), quartz (~35 vol%), plagioclase (~20 vol%), and biotite (~10 vol%), with minor apatite, zircon, and allanite (fig. 3d).

Mafic microgranular enclaves are widespread in the porphyritic granite body. They generally form

ovoid bodies with the long axis ranging from several centimeters up to 40 cm (fig. 3e, 3g). The enclaves are grayish black in hand specimen. They show a microcrystalline texture (fig. 3f, 3h) containing pyroxene (~5 vol%), amphibole (~10 vol%), biotite (~15 vol%), plagioclase (~20 vol%), K-feldspar (30 vol%), and quartz (~20 vol%). Large K-feldspar crystals often crosscut the enclave-host boundary and also occur inside the enclaves (fig. 3e, 3g). The K-feldspar crystals within MMEs worldwide are generally regarded as xenocrysts captured from the partially crystalline host magma by the enclave magma (Vernon et al. 1988; Perugini et al. 2003). Apatite crystals in the MMEs are elongated (fig. 3h), which suggests that they formed during rapid cooling (e.g., Sparks and Marshall 1986).

### Sampling and Analytical Methods

**Sampling.** Fresh samples for this study were collected from surface exposures and open pits, and the main sample locations are shown in figure 2. The lava samples containing the fewest lithic fragments were chosen for whole-rock analyses. Twenty-seven samples (seven for lava, 10 for granite, and 10 for MMEs) were crushed to 200-mesh with an agate mill for whole-rock geochemical analysis.

**Zircon U-Pb Dating.** Zircon grains separated from three samples (YSHV-01 from the lava, YHSV-50 from the granite, and YHSV-48 from the MMEs

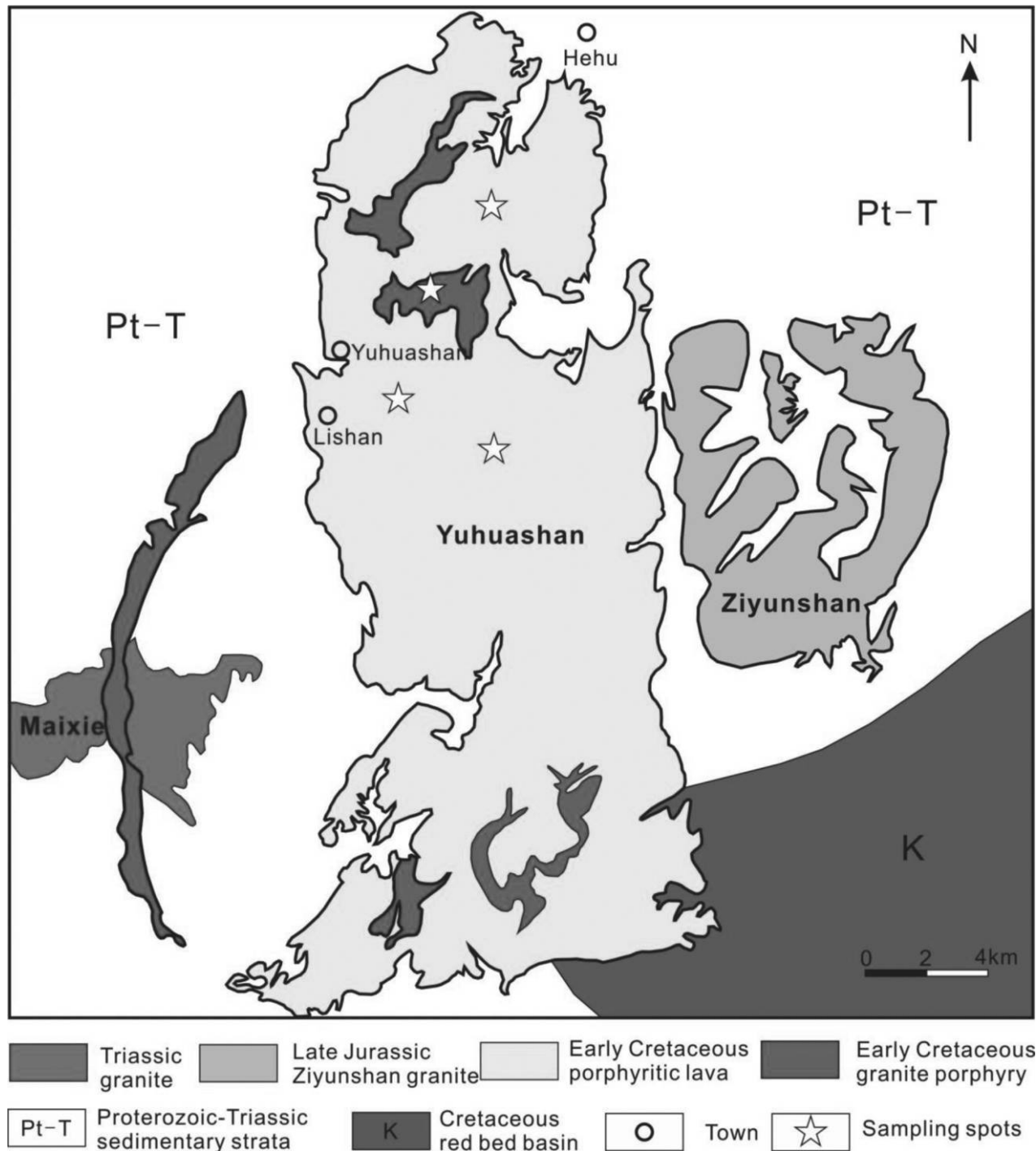


**Figure 2.** Simplified geological map of the Yuhuashan Complex. A color version of this figure is available online.

hosted by the granite) were mounted in epoxy resin and polished to approximately half their thickness. The internal structures were examined, with the cathodoluminescence (CL) imaging technique, with a scanning electron microprobe at the State Key Laboratory of Continental Dynamics at Northwest University, China.

In situ zircon U-Pb analyses were carried out with a GeoLasPro laser ablation (LA) system attached to an Agilent 7700x ICP-MS at the State Key Laboratory of Ore Deposit Geochemistry, Institute of Geochemistry, Chinese Academy of Science, Guiyang. The ablation protocol employed a spot diameter of 32  $\mu\text{m}$  at a 5-Hz repetition rate for

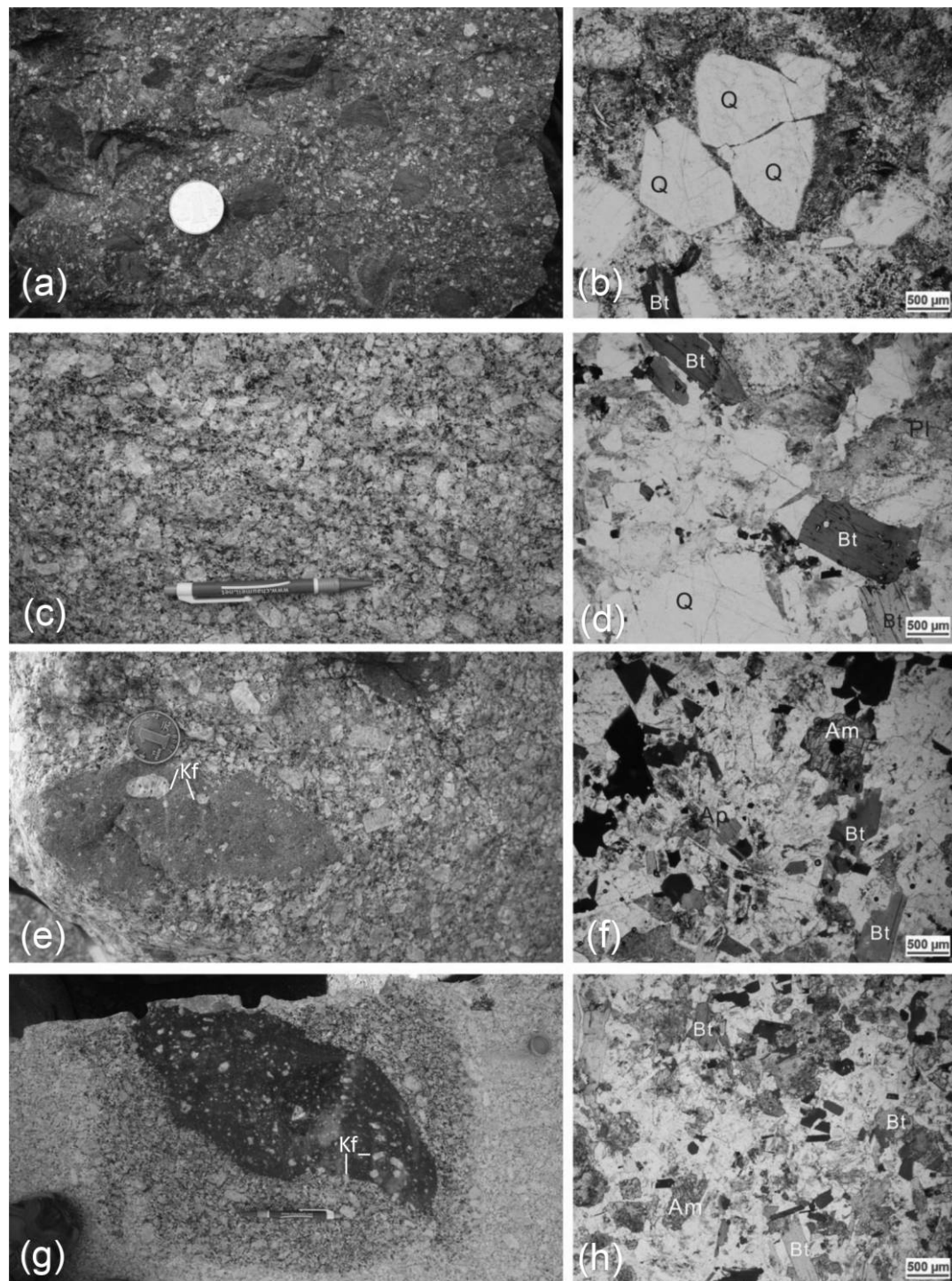


**Figure 3.** Photographs of representative volcanic rocks, porphyritic granite, and mafic microgranular enclaves (MMEs) from the Yuhuashan Complex: *a, b*, porphyritic lava; *c, d*, porphyritic granite; *e-h*, the MMEs. The diameter of the coin in *a* and *e* is 2.5 cm. The length of the pen in *c* and *g* is about 15 cm. Am = amphibole; Ap = apatite; Bt = biotite; Kf = K-feldspar; Pl = plagioclase; Q = quartz. A color version of this figure is available online.

40 s. Helium was used as a carrier gas to efficiently transport the aerosol. Zircon 91500 (1064 Ma; Wiedenbeck et al. 2004) was used as an external standard to correct for elemental fractionation, while the zircon standard Plešovice was used for quality control. Common-Pb correction was calculated with the method of Andersen (2002). Data reduction was performed off-line with the ICPMSDataCal software (Liu et al. 2010a, 2010b). The Plešovice zircon yields an average age of  $339 \pm 4$  Ma ( $2\sigma$ ,  $n = 14$ ), similar to the reference age (337 Ma; Sláma et al. 2008).

**Major- and Trace-Element Contents of Whole-Rock Samples.** Major-element contents of whole-rock samples were determined with an X-ray fluorometer (ARL-9800) at Modern Analysis Center of Nanjing University. The analytical uncertainties for most major elements are better than 0.5%.

Trace-element contents were determined with a Finnigan MAT Element II high-resolution ICP-MS at the State Key Laboratory for Mineral Deposit Research at Nanjing University. The instrument settings and analytical method are the same as described in Gao et al. (2003). The analytical uncertainties for most elements are better than 5%.

**Sr-Nd Isotopic Compositions of Whole-Rock Samples.** Determination of Sr and Nd isotopic composition was carried out with a Finnigan MAT Triton TI TIMS at the State Key Laboratory for Mineral Deposit Research, Nanjing University. The analytical method is described in Pu et al. (2005). A decay constant for  $^{147}\text{Sm}$  ( $6.54 \times 10^{-12} \text{ y}^{-1}$ ; Lugmair and Marti 1978), the chondritic values of  $^{143}\text{Nd}/^{144}\text{Nd}$  (0.512638) and  $^{147}\text{Sm}/^{144}\text{Nd}$  (0.1967; Jacobsen and Wasserburg 1980), the depleted-mantle values of  $^{143}\text{Nd}/^{144}\text{Nd}$  (0.513151) and  $^{147}\text{Sm}/^{144}\text{Nd}$  (0.2136), and a mean crustal value of  $^{147}\text{Sm}/^{144}\text{Nd}$  (0.118; Jahn and Condie 1995) were adopted for calculation of  $\varepsilon_{\text{Nd}}(t)$  values and two-stage model ages.

**Zircon Lu-Hf Isotopic Compositions.** Zircon Hf isotope analysis was carried out in situ with a New Wave UP 193-nm LA system attached to a Neptune Plus multicollector ICP-MS at the State Key Laboratory of Mineral Deposits Research at Nanjing University. Zircon grains selected for Hf isotopic analyses had been previously analyzed for U-Pb dating. The spots for Hf isotope analyses were selected near the spots for U-Pb analyses or on the other side of the same grain. The Yb and Lu mass bias correction protocols details are as described by Wu et al. (2006). The mean  $\beta_{\text{Yb}}$  and  $\beta_{\text{Hf}}$  values of the individual analytical spots were applied for in situ analysis correction. Zircon 91500 was used as the reference standard, yielding an average  $^{176}\text{Hf}/$

$^{177}\text{Hf}$  of  $0.282295 \pm 0.000029$  ( $2\sigma$ ,  $n = 25$ ) in this study. A depleted-mantle model with  $^{176}\text{Hf}/^{177}\text{Hf} = 0.28325$  and  $^{176}\text{Lu}/^{177}\text{Hf} = 0.0384$  (Nowell et al. 1998) and a chondritic model with  $^{176}\text{Hf}/^{177}\text{Hf} = 0.282772$  and  $^{176}\text{Lu}/^{177}\text{Hf} = 0.0332$  (Blichert-Toft and Albarède 1997) were used to calculate  $\varepsilon_{\text{Hf}}(t)$  values and model ages.

## Results

**Zircon U-Pb Ages.** *Yuhuashan Porphyritic Lava (YHSV-01).* Zircon grains from the Yuhuashan porphyritic lava sample YHSV-01 (location:  $27^{\circ}53'02''\text{N}$ ,  $115^{\circ}42'07''\text{E}$ ) are euhedral crystals with a length of 150–200  $\mu\text{m}$  and a width of 50–100  $\mu\text{m}$ , yielding length-width ratios that mostly vary from 2:1 to 4:1. Most of the zircons display homogenous cores and concentric zoning in the rim in CL images (fig. 4a), suggesting a magmatic origin (Hoskin and Schaltegger 2003; Wu and Zheng 2004).

Twenty-three spot analyses were carried out on 23 zircon grains, and the U-Pb age data are listed in table S1 (tables S1–S4 are available online). U concentrations of these analyses vary from 113 to 923 ppm, and Th concentrations vary from 59.4 to 241 ppm. Th/U values vary from 0.26 to 0.62. Two spots show relatively older ages ( $\sim 155$  Ma). The other 21 spots display consistent  $^{206}\text{Pb}/^{238}\text{U}$  ages in the range of 131–144 Ma, giving a weighted average age of  $136 \pm 2$  Ma ( $n = 21$ , MSWD = 14; fig. 4a). The relatively large MSWD value is caused by the very small internal error ( $\sim 1\%$ ) for individual spot analyses. If we adopted the external error ( $\sim 2.5\%$ ) as the individual spot error, the weighted average age would be  $136 \pm 2$  Ma ( $n = 21$ , MSWD = 1.4). This age is the best estimate of the formation age of the Yuhuashan porphyritic lava.

*Yuhuashan Porphyritic Granite (YHSV-50).* Zircon grains from the Yuhuashan porphyritic granite sample YSHV-50 (location:  $27^{\circ}48'08''\text{N}$ ,  $115^{\circ}36'32''\text{E}$ ) are euhedral and elongated. Most of the zircon grains have a length of 150–200  $\mu\text{m}$  and a width of 50–100  $\mu\text{m}$ , with length-width ratios varying from 2:1 to 4:1. In CL images, they generally display homogenous cores and concentric zoning in the rim (fig. 4b).

Twenty-three spot analyses yield U concentrations that vary from 206 to 1103 ppm and Th concentrations from 93.4 to 391 ppm. Th/U values vary from 0.22 to 0.62. All 23 spots display consistent  $^{206}\text{Pb}/^{238}\text{U}$  ages of 130–144 Ma and give a weighted average age of  $135 \pm 2$  Ma ( $n = 23$ , MSWD = 10). This age is the best estimate of the emplacement age of the Yuhuashan porphyritic granite.

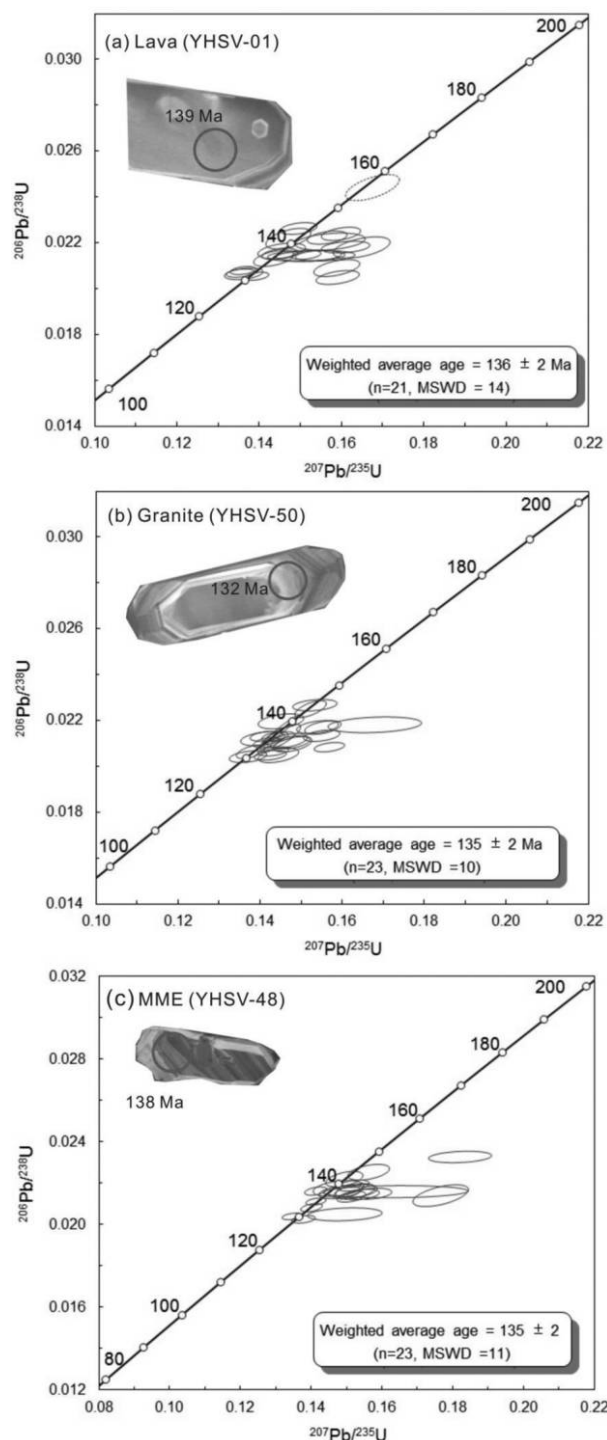


**Figure 4.** Laser ablation ICP-MS zircon U-Pb concordia diagrams for the porphyritic lava (a), the porphyritic granite (b), and the mafic microgranular enclaves (MMEs; c) from the Yuhuashan Complex. The dashed oval indicates an inherited grain. A color version of this figure is available online.

*MMEs (YHSV-48).* Sample YHSV-48 (location: 27°48'08"N, 115°36'32"E) was collected from an MME in the Yuhuashan porphyritic granite. Zircon grains are smaller than those from the host granite (YHSV-50). Most of the zircon grains have a length of 50–150  $\mu\text{m}$  and a width of 50–100  $\mu\text{m}$ , yielding length-width ratios from 1:1 to 2:1. They also show clear oscillatory zoning in CL images, implying that they formed during magmatic crystallization (fig. 4c).

Twenty-three spot analyses were performed, and they yield U concentrations varying from 145 to 858 ppm and Th concentrations from 72.0 to 300 ppm. Th/U values vary from 0.32 to 1.10. The  $^{206}\text{Pb}/^{238}\text{U}$  ages vary from 129 to 144 Ma and yield a weighted average age of  $135 \pm 2$  Ma ( $n = 23$ , MSWD = 11). This age is consistent with that of the host granite.

**Geochemical and Isotopic Data.** *Yuhuashan Porphyritic Lava.* Major- and trace-element contents of the studied samples are listed in table S2. The volcanic rocks are classified as rhyolite, dacite, and trachydacite, according to the total alkaline–silica (TAS) diagram of Le Bas et al. (1986; fig. 5). The A/CNK (molar ratio  $\text{Al}_2\text{O}_3/(\text{CaO} + \text{Na}_2\text{O} + \text{K}_2\text{O})$ ) values vary from 0.97 to 1.09, indicating that the lava is metaluminous to weakly peraluminous (fig. 6). There is a general decrease in  $\text{TiO}_2$ ,  $\text{Al}_2\text{O}_3$ ,  $\text{Fe}_2\text{O}_3$ ,  $\text{MgO}$ ,  $\text{CaO}$ , and  $\text{P}_2\text{O}_5$  with increasing  $\text{SiO}_2$ , whereas  $\text{K}_2\text{O}$  and  $\text{Na}_2\text{O}$  have relatively constant abundances (fig. 7). The studied samples have high alkali contents ( $\text{K}_2\text{O} = 4.71\%–5.28\%$ ,  $\text{Na}_2\text{O} = 2.66\%–3.51\%$ ). In the plot of alkalinity ratio versus  $\text{SiO}_2$ , all the samples plot in the alkaline field (fig. 8).

The Yuhuashan porphyritic lava has high Zr contents (239–463 ppm), yielding zircon saturation temperatures of 814°C–874°C based on the equation of Watson and Harrison (1983). On variation diagrams of  $\text{SiO}_2$  versus selected trace elements (fig. 9), the samples show a general decrease of Sr, Ba, Sc, and V with increasing  $\text{SiO}_2$  and considerable scatter for Rb, Zr, Y, and Nb.

On a primitive mantle–normalized trace-element spider diagram, the lava shows relative depletion in Ba, Nb, Ta, Sr, Eu, and Ti (fig. 10a). The depletions of Nb and Ta are similar to those seen in arc magmatic rocks (e.g., Kelemen et al. 2003). The lava has high rare earth element (REE) contents (222–391 ppm). Chondrite-normalized REE patterns of the lava show an enrichment in light REEs (LREEs), with  $(\text{La}/\text{Yb})_N$  values of 14.7–16.9, and slightly negative Eu anomalies, with  $\text{Eu}/\text{Eu}^*$  values of 0.47–0.64 (fig. 11a).

The whole-rock Sr–Nd isotopic data are listed in table S3. The initial  $^{87}\text{Sr}/^{86}\text{Sr}$  ( $(^{87}\text{Sr}/^{86}\text{Sr})_i$ ) and  $\epsilon_{\text{Nd}}(t)$

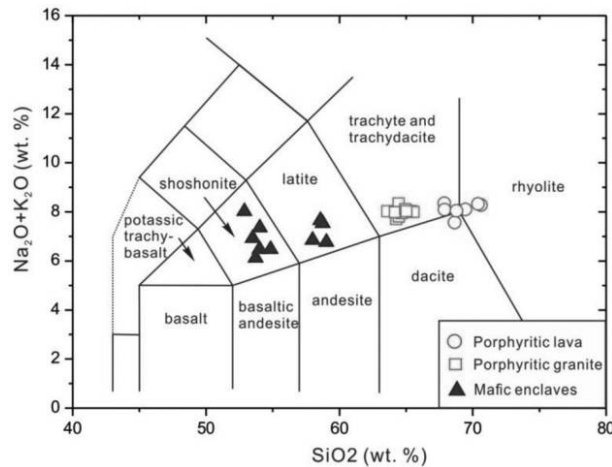


**Figure 5.** Total alkali–silica diagram for the Yuhuashan Complex and its mafic microgranular enclaves (after Le Bas et al. 1986). A color version of this figure is available online.

values of the porphyritic lava samples have been calculated at 136 Ma. Calculated  $(^{87}\text{Sr}/^{86}\text{Sr})_i$  values vary from 0.70953 to 0.71127. The calculated  $\varepsilon_{\text{Nd}}(t)$  values vary from  $-8.1$  to  $-7.6$ , and two-stage model ages vary from 1.55 to 1.59 Ga.

Twenty-four spots on zircon grains from sample YHSV-01 were analyzed for Lu–Hf isotopic compositions, and the results are listed in table S4. The initial  $^{176}\text{Hf}/^{177}\text{Hf}$  and  $\varepsilon_{\text{Hf}}(t)$  values of the samples have been calculated at 136 Ma. The initial  $^{176}\text{Hf}/^{177}\text{Hf}$  vary from 0.282402 to 0.282505. The calculated  $\varepsilon_{\text{Hf}}(t)$  values vary from  $-10.8$  to  $-6.4$ , with an average value of  $-8.8$  (fig. 12a). The two-stage Hf isotopic model ages vary from 1.59 to 1.87 Ga, with an average model age of 1.74 Ga (fig. 12b).

**Yuhuashan Porphyritic Granite.** The Yuhuashan porphyritic granite samples have lower  $\text{SiO}_2$  contents than the porphyritic lava (table S2; fig. 7). They have relatively higher  $\text{Al}_2\text{O}_3$ ,  $\text{TiO}_2$ ,  $\text{MgO}$ ,  $\text{CaO}$ , and  $\text{P}_2\text{O}_5$  contents. The A/CNK values vary from 0.95 to 1.01 (fig. 5), and most samples are metaluminous (fig. 6). In the variation diagram of  $\text{SiO}_2$  versus major elements (fig. 7), the granite samples show a general linear trending with the porphyritic lava samples for  $\text{TiO}_2$ ,  $\text{Al}_2\text{O}_3$ ,  $\text{MgO}$ , and  $\text{P}_2\text{O}_5$ . The samples fall on the boundary between alkaline and calc-alkaline granites on the plot of alkalinity ratio versus  $\text{SiO}_2$  (fig. 8).

The Yuhuashan porphyritic granite has lower Rb contents, higher Sr contents, and higher Ba contents than the lava (fig. 9). The Yuhuashan porphyritic granite has also higher Zr contents (410–529 ppm), yielding zircon saturation temperatures of  $854^\circ$ – $876^\circ\text{C}$ .

In a primitive mantle–normalized trace-element spider diagram (fig. 10b), the granite shows depletions in Ba, Nb, Ta, Sr, and Ti that are smaller than those observed in the lava. Total REE contents vary from 257 to 340 ppm. Chondrite-normalized REE patterns of the granite show enrichment in LREEs, with  $(\text{La}/\text{Yb})_N$  values of 17.6–22.9, and slightly negative Eu anomalies with  $\text{Eu}/\text{Eu}^*$  values of 0.66–0.78 (fig. 11b). The LREE enrichments are larger than those observed in the lava, but the negative anomalies of Eu are smaller.

The  $(^{87}\text{Sr}/^{86}\text{Sr})_i$  and  $\varepsilon_{\text{Nd}}(t)$  values of the porphyritic granite samples have been calculated at 135 Ma (table S3). Calculated  $(^{87}\text{Sr}/^{86}\text{Sr})_i$  values vary from 0.71046 to 0.71122. The  $\varepsilon_{\text{Nd}}(t)$  values vary from  $-8.0$  to  $-7.4$ , and two-stage model ages vary from 1.53 to 1.58 Ga.

Twenty-two spots on zircon grains from sample YHSV-50 were analyzed for Lu–Hf isotopic compositions (table S4). The calculated  $\varepsilon_{\text{Hf}}(t)$  values vary from  $-9.9$  to  $-7.0$ , with an average value of  $-8.7$  (fig. 12c). The two-stage Hf isotopic model ages vary from 1.63 to 1.81 Ga, with an average age of 1.73 Ga (fig. 12d). Whole-rock Nd and zircon Hf isotopic compositions of the granite are similar to those of the lava.

**MMEs.** The MME samples have lower  $\text{SiO}_2$  and higher  $\text{TiO}_2$ ,  $\text{MgO}$ ,  $\text{Fe}_2\text{O}_3$ , and  $\text{CaO}$  contents than either of the Yuhuashan rock types (fig. 7). They also have high  $\text{Mg}/(\text{Mg}+\text{Fe})$  (0.44–0.58). The MME samples have high  $\text{K}_2\text{O}$  contents (3.19%–4.75%), and in the TAS diagram (fig. 5) the mafic enclaves plot in the fields of shoshonite and latite, corre-

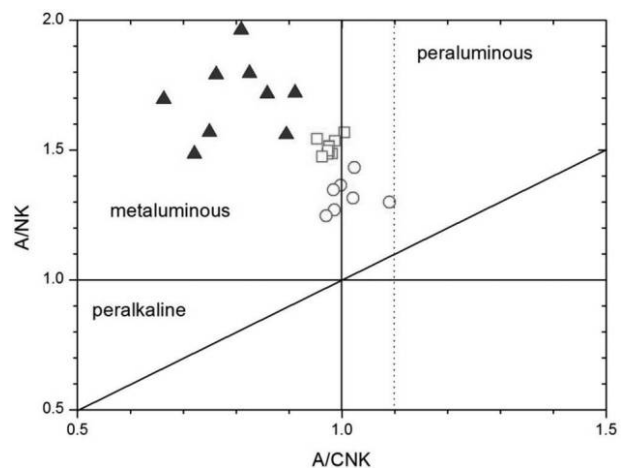


**Figure 6.** Plot of A/CNK (molar ratio  $\text{Al}_2\text{O}_3/(\text{CaO} + \text{Na}_2\text{O} + \text{K}_2\text{O})$ ) versus A/NK (molar ratio  $\text{Al}_2\text{O}_3/(\text{Na}_2\text{O} + \text{K}_2\text{O})$ ) for the Yuhuashan Complex and its mafic microgranular enclaves. Symbols are as in figure 5. A color version of this figure is available online.

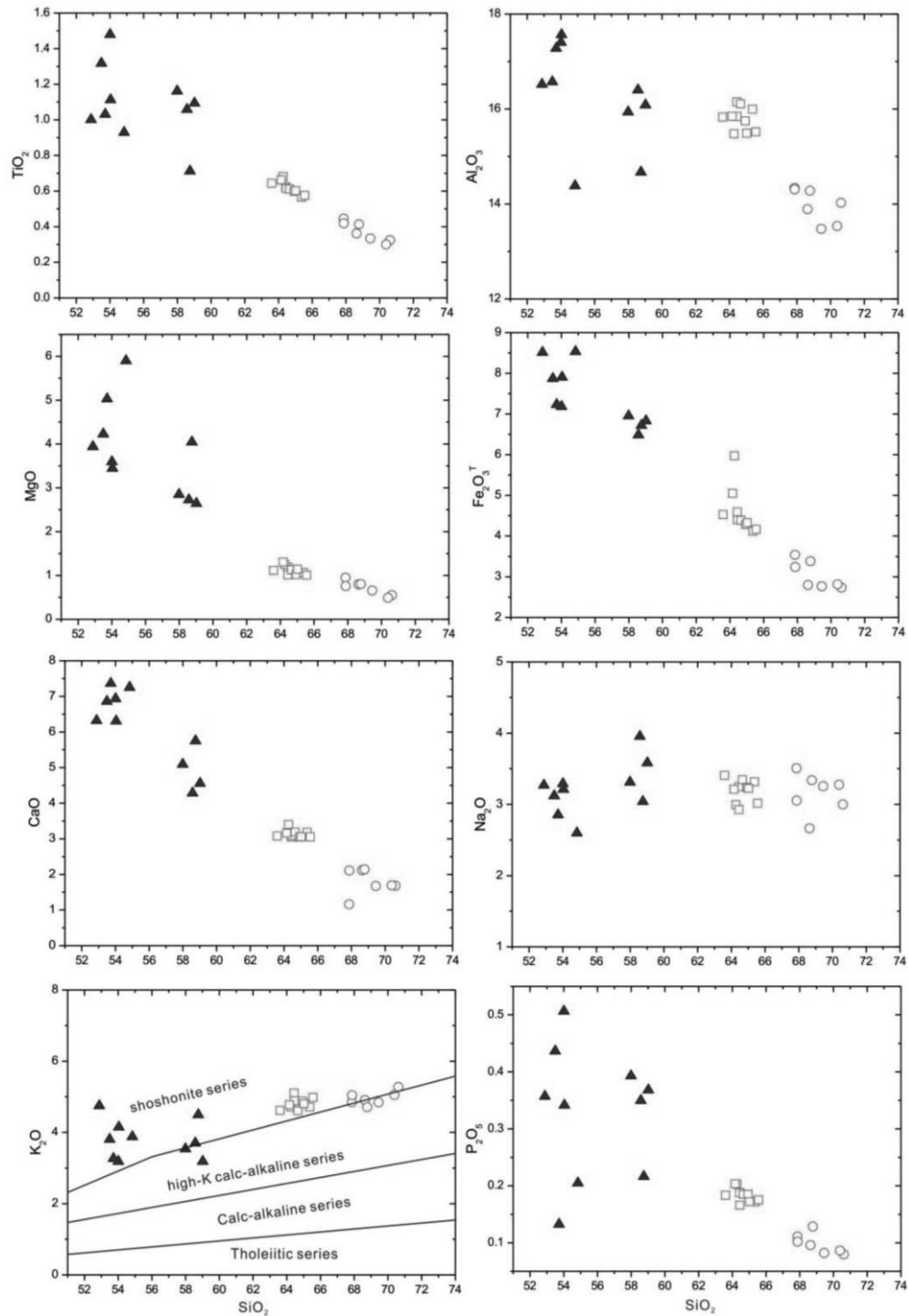


**Figure 7.** Plots of selected major oxides (wt%) versus  $\text{SiO}_2$  (wt%) for the Yuhuashan Complex and its mafic microgranular enclaves. Symbols are as in figure 5. A color version of this figure is available online.

sponding to the (quartz) monzonite compositions of the quartz-alkali-plagioclase diagram.

The MME samples have higher compatible trace-element contents (e.g., 18.83–35.19 ppm for Sc and 167–279 ppm for V) than the host granite (fig. 9). Rb

contents vary from 129 to 219 ppm, and Sr contents vary from 263 to 529 ppm. The MMEs have Zr contents of 174–328 ppm.

In a primitive mantle-normalized trace-element spider diagram (fig. 10c), the MMEs show slight

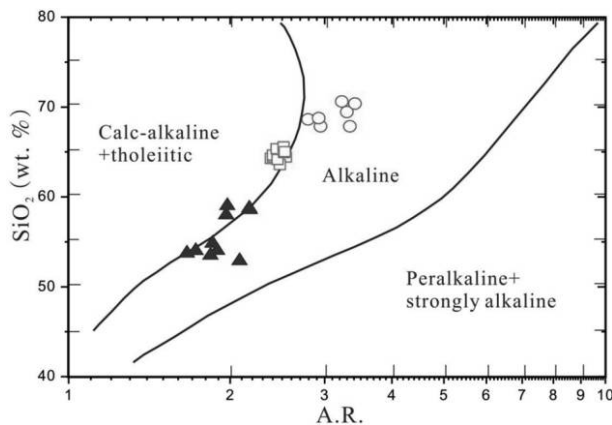


**Figure 8.** Plot of alkalinity ratio (A.R.) versus  $\text{SiO}_2$  for the Yuhuashan Complex and its mafic microgranular enclaves, where  $\text{A.R.} = [\text{Al}_2\text{O}_3 + \text{CaO} + (\text{Na}_2\text{O} + \text{K}_2\text{O})] / [\text{Al}_2\text{O}_3 + \text{CaO} - (\text{Na}_2\text{O} + \text{K}_2\text{O})]$  (wt%). Symbols are as in figure 5. A color version of this figure is available online.

depletions in Ba, Nb, Ta, Sr, and Ti and are similar to continental arc andesites (fig. 10c; Kelemen et al. 2003). Total REE contents vary from 161 to 236 ppm. Chondrite-normalized REE patterns of the MMEs show enrichment in LREEs, with  $(\text{La}/\text{Yb})_{\text{N}}$  values of 6.74–14.2 (fig. 11c).

The  $(^{87}\text{Sr}/^{86}\text{Sr})_i$  and  $\varepsilon_{\text{Nd}}(t)$  values of the MMEs samples have been calculated at 135 Ma (table S3). Calculated  $(^{87}\text{Sr}/^{86}\text{Sr})_i$  values vary from 0.70823 to 0.71032. The  $\varepsilon_{\text{Nd}}(t)$  values vary from  $-7.1$  to  $-5.1$ , and two-stage model ages vary from 1.35 to 1.51 Ga. The  $\varepsilon_{\text{Nd}}(t)$  values are higher than those of the host granite samples.

Twenty spots on zircon grains from sample YHSV-48 were analyzed for Lu-Hf isotopic compositions (table S4). The MME samples show higher  $\varepsilon_{\text{Hf}}(t)$  values and lower  $T_{\text{DM}^c}$  model ages than the porphyritic lava and granite (fig. 12). Calculated  $\varepsilon_{\text{Hf}}(t)$  values vary from  $-10.3$  to  $-2.1$ , with an average value of  $-6.1$  (fig. 12e). The two-stage Hf isotopic model ages vary from 1.32 to 1.83 Ga, with an average age of 1.57 Ga (fig. 12f).

## Discussion

**Petrogenetic Type of the Yuhuashan Complex.** The term “A-type granite” was first introduced to distinguish a group of alkaline, anorogenic, and anhydrous granites (Loiselle and Wones 1979). A-type granite generally exhibits specific geochemical characteristics, such as high alkali metal contents, high  $\text{FeO}^{\text{T}}/\text{MgO}$ , high high-field-strength-element (HFSE) contents ( $\text{Zr} > 250$  ppm and  $\text{Zr} + \text{Nb} + \text{Ce} + \text{Y} > 350$  ppm), high REE contents, and high

$\text{Ga}/\text{Al}$  ( $10,000 \times \text{Ga}/\text{Al} > 2.6$ ; Whalen et al. 1987; King et al. 2001; Bonin 2007). The Yuhuashan lava and porphyritic granite show all these A-type geochemical characteristics: high total alkali contents ( $\text{Na}_2\text{O} + \text{K}_2\text{O} = 7.57\%–8.35\%$ ), high  $\text{FeO}^{\text{T}}/\text{MgO}$  (3.15–4.47), high contents of HFSEs ( $\text{Zr} + \text{Nb} + \text{Ce} + \text{Y} = 384–711$  ppm), and high  $10,000 \times \text{Ga}/\text{Al}$  (2.30–3.22). In the relevant classification diagrams (Whalen et al. 1987), all the samples plot in the A-type field (fig. 13). The high Rb/Nb and Y/Nb of these rocks further suggest that they belong to the  $\text{A}_2$  group of Eby (1992; fig. 14), which represents magma derived from postcollisional tectonic settings or anorogenic environments.

The  $\text{Al}_2\text{O}_3/\text{TiO}_2$  values of granitic partial melts are thought to be a function of melting temperature (Jung and Pfänder 2007). The relatively low  $\text{Al}_2\text{O}_3/\text{TiO}_2$  values (23–45) for the Yuhuashan Complex indicate that their sources were partially melted under high-temperature conditions. Inherited zircon grains are rare in the Yuhuashan Complex, a feature of most A-type granites (Williams 1992). The magma temperatures calculated by zircon saturation thermometry (Miller et al. 2003) for the Yuhuashan Complex vary from  $814^\circ$  to  $876^\circ\text{C}$ , higher than those of common I- and S-type granites (usually lower than  $800^\circ\text{C}$ ).

More and more Early Cretaceous A-type volcanic rocks and granites along the GHVB have been identified in the past decade (fig. 1; table 1). These rocks share similar A-type geochemical characteristics—for example, high total alkali contents, enrichment in HFSEs, and high Ga/Al (fig. 13)—and they all have high Y/Nb and Rb/Nb that place them in the  $\text{A}_2$  subtype of Eby (1992; fig. 14). Together, these rocks form an Early Cretaceous NNE-trending,  $\text{A}_2$ -type magmatic rock belt along the GHVB that was emplaced in a short duration of 137–122 Ma.

**Magma Sources of the Yuhuashan Complex.** The Yuhuashan lava and granite have lower  $\varepsilon_{\text{Nd}}(t)$  values ( $-8.1$  to  $-7.4$ ) and zircon  $\varepsilon_{\text{Hf}}(t)$  values (approx.  $-8.8$ ) than coeval mantle-derived magmas resembling the MMEs ( $\varepsilon_{\text{Nd}}(t)$ :  $-7.2$  to  $-5.4$ ;  $\varepsilon_{\text{Hf}}(t)$ : approx.  $-6.1$ ), which therefore rules out extensive fractional crystallization from a coeval mafic magma for the origin of the Yuhuashan Complex. The  $\varepsilon_{\text{Nd}}(t)$  values of the Yuhuashan Complex are higher than those of the early and middle Proterozoic parametamorphic rocks but lower than those of the orthometamorphic rocks at the eruption time (fig. 15). This could be taken to suggest that the Yuhuashan Complex was derived from partial melting at depth of an early-to-middle Proterozoic terrain that included both orthometamorphic and parametamorphic rocks. An

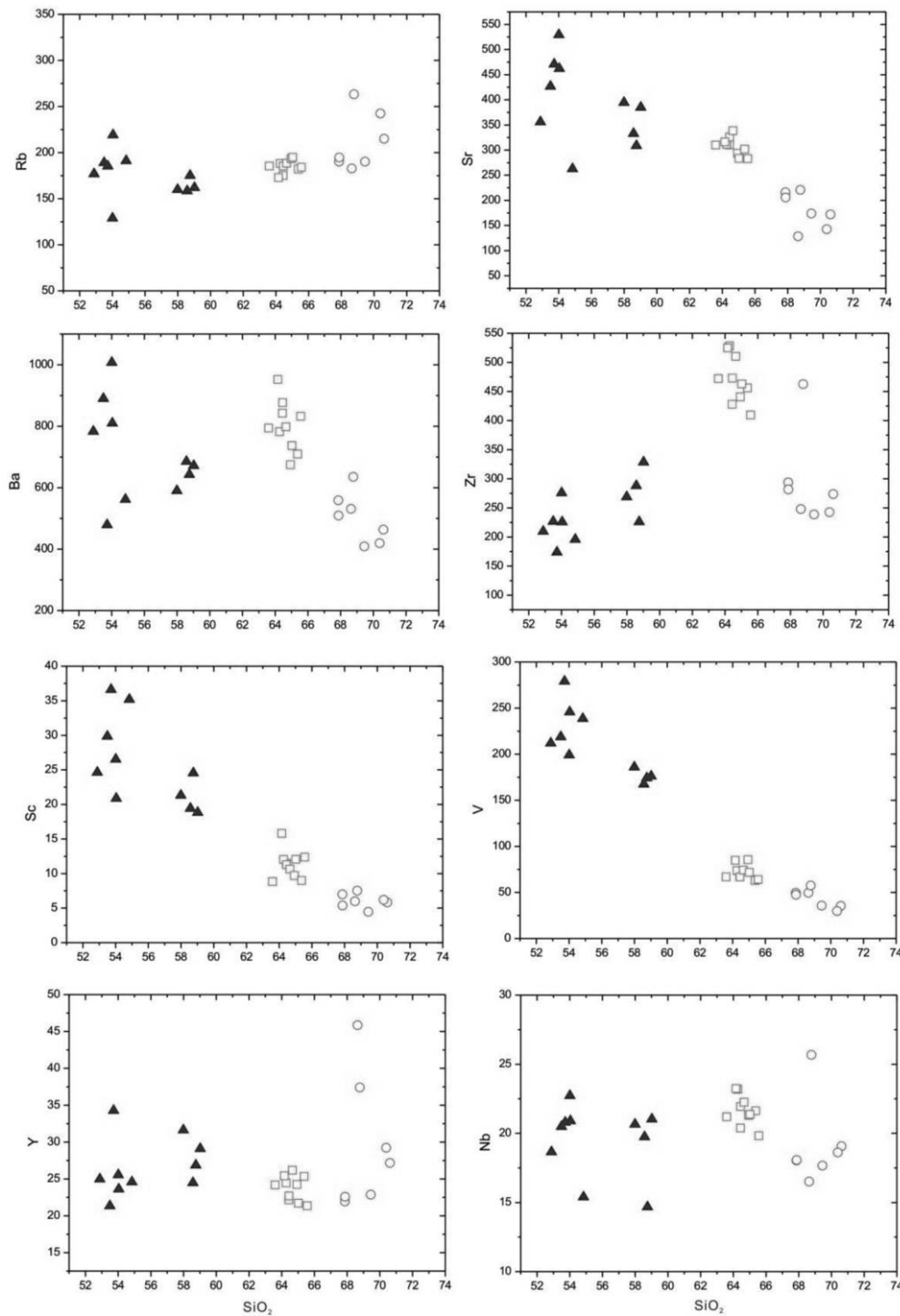


**Figure 9.** Plots of selected trace elements (ppm) versus  $\text{SiO}_2$  (wt%) for the Yuhuashan Complex and its mafic microgranular enclaves. Symbols are as in figure 5. A color version of this figure is available online.

isotopic modeling of two-end-member component mixing was conducted, and the results are shown in figure 15. About a 30%–40% orthometamorphic rock fraction is necessary to generate the isotopic compositional range of the Yuhuashan Complex.

However, both types of metamorphic rocks generally have  $(^{87}\text{Sr}/^{86}\text{Sr})_i$  values higher than those of the Yuhuashan Complex (fig. 15), and we cannot, therefore, rule out a contribution from underplated mafic magma to the magmas of the Yuhuashan Complex.

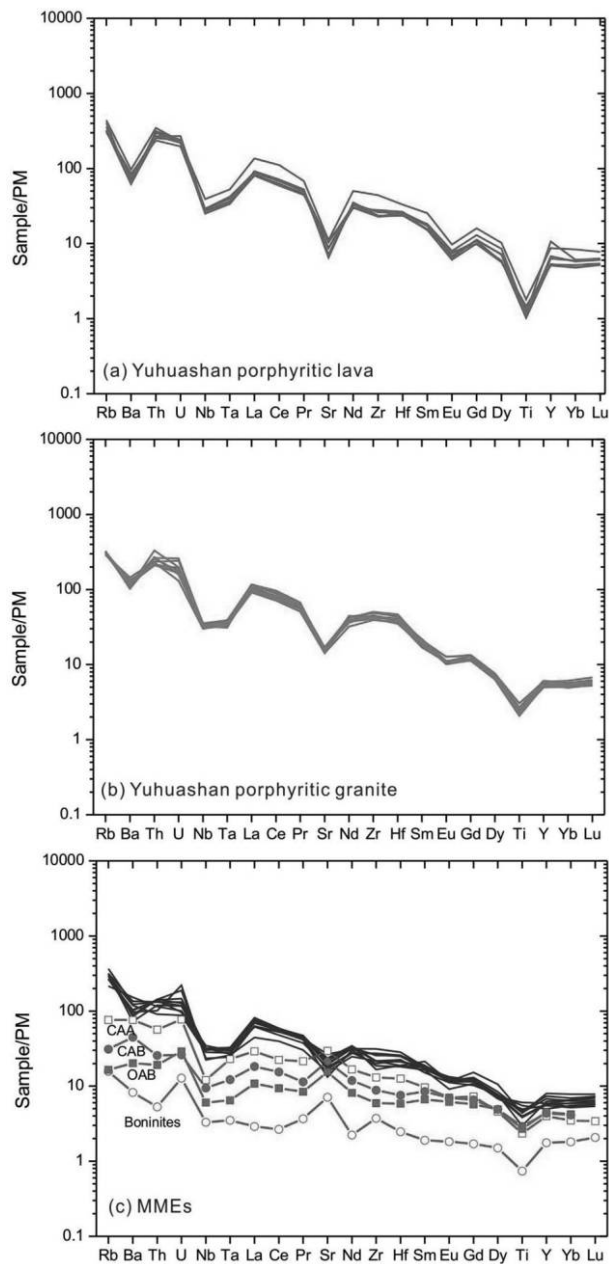


**Figure 10.** Primitive mantle (PM)-normalized trace element spidergrams for the Yuhuashan Complex and its mafic microgranular enclaves (MMEs). The normalization values of the PM are from Sun and McDonough (1989). The average data of CAA (continental arc andesites), CAB (continental arc basalts), OAB (oceanic arc basalts), and boninites come from Kelemen et al. (2003). A color version of this figure is available online.

The nearby Xiangshan A-type volcanic rocks (135–137 Ma) and the Shenyan tuff (135–137 Ma) in the GHVB have Sr-Nd-Hf isotopic compositions similar to those of the Yuhuashan Complex, and it has been suggested that they were derived mainly

from partial melting of Proterozoic crust without significant additions of mantle-derived magma (e.g., Jiang et al. 2005; Yang et al. 2011; Shu et al. 2017). However, the Tongshan (129 Ma), Damaoshan (122–126 Ma), Baijuehajian (126 Ma), Miaohou and Shanhou (127–130 Ma), and Furongshan A-type

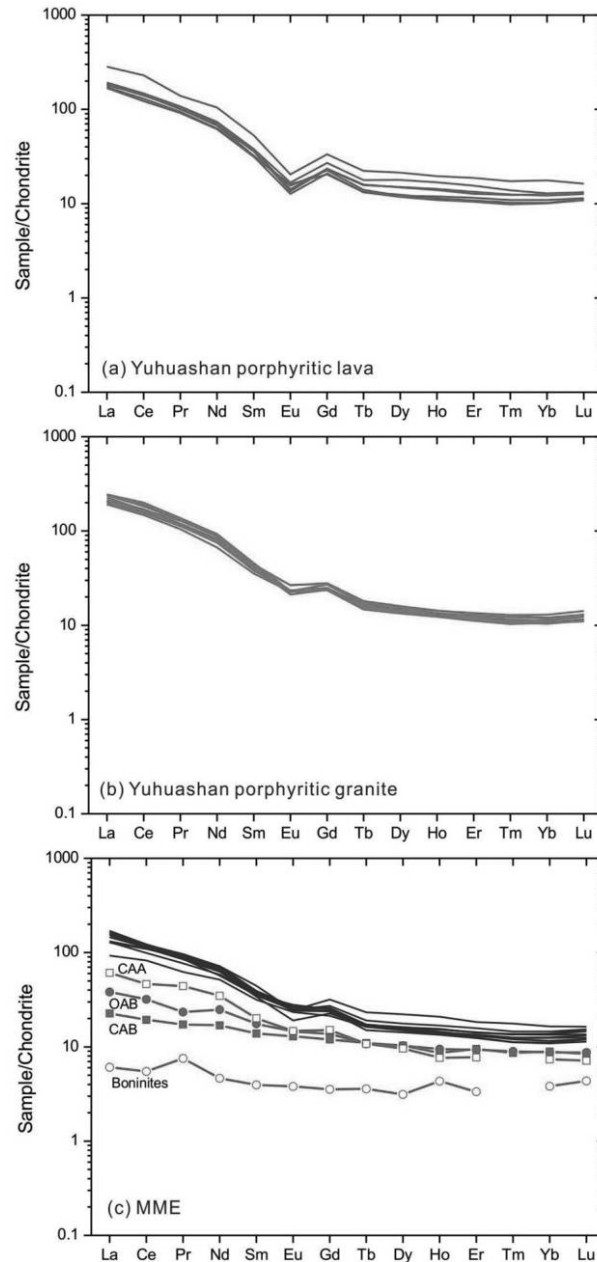


**Figure 11.** Chondrite-normalized rare earth element diagrams for the Yuhuashan Complex and its mafic microgranular enclaves (MME). The normalization values of chondrite are from Boynton (1984). The average data of CAA (continental arc andesites), CAB (continental arc basalts), OAB (oceanic arc basalts), and boninites come from Kelemen et al. (2003). A color version of this figure is available online.

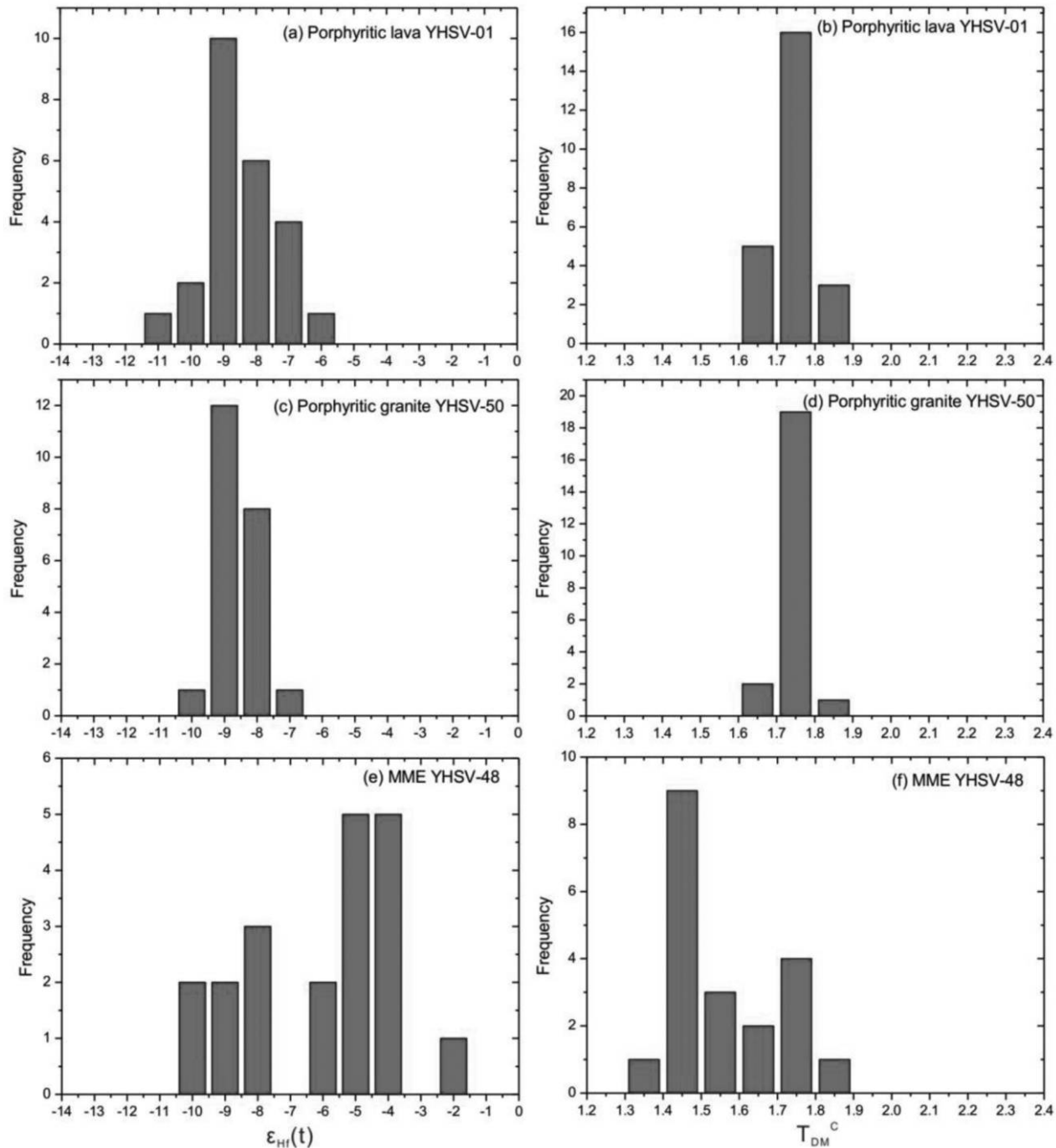


**Figure 12.** Histograms of zircon  $\epsilon_{\text{Hf}}(t)$  values and two-stage model ages ( $T_{\text{DM}}^c$ ) of the Yuhuashan Complex and the mafic microgranular enclaves (MME). A color version of this figure is available online.

granites all have significantly higher  $\epsilon_{\text{Nd}}(t)$  values (table 1) than the Yuhuashan Complex, implying that these complexes do contain an input of juvenile mantle melt (e.g., Wong et al. 2009; Yang et al. 2012; Wang et al. 2015; Xia et al. 2016).

**Origin of MMEs.** Mafic microgranular enclaves are widespread in granitic rocks and have been the

focus of many studies (e.g., Didier and Barbarin 1991), but different models have been proposed to explain their origin. For example, MMEs have been suggested to be (1) restites of source rocks (Chappell et al. 1987; White et al. 1999); (2) wall-rock xenoliths (Maas et al. 1997); (3) early crystal-melt segregations (Dahlquist 2002; Donaire et al. 2005);

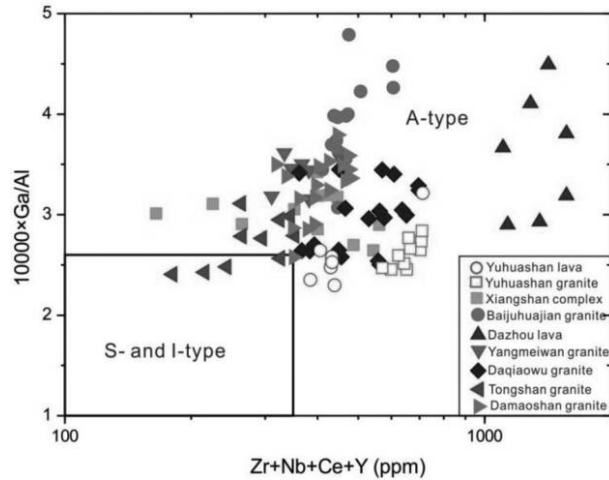


**Figure 13.** The  $(10,000 \times \text{Ga}/\text{Al})$ -versus- $(\text{Zr} + \text{Nb} + \text{Ce} + \text{Y})$  classification diagram of Whalen et al. (1987) for the Early Cretaceous volcanic rocks and granites in the Gan-Hang Belt. Data sources: this study for the Yuhuashan Complex; Jiang et al. (2005) for the Xiangshan Complex; Wong et al. (2009) for the Baijuehuajian granite; Yang et al. (2013) for the Dazhou lava; Yang et al. (2012) for the Yangmeiwan and Daqiaowu granites; and Jiang et al. (2011) for the Tongshan and Damaoshan granites. A color version of this figure is available online.

or (4) products of mingling of basaltic and felsic magmas (Allen 1991; Barbarin 2005; Perugini et al. 2003; Vernon 1984; Zhao et al. 2010, 2012).

The MMEs in the Yuhuashan porphyritic granite have igneous microtextures (fig. 3*d*), suggesting a magmatic origin. The presence of K-feldspar megacrysts in the enclaves also supports that the enclaves were hybrids when they formed. This is further reinforced by the observation that the zircons from the enclaves yield the same U-Pb age as the host granite (fig. 4). Hence, these observations constitute direct evidence against the possibility that these enclaves are restites or xenoliths.

Mafic enclaves can be formed by early crystal-liquid differentiation mechanisms operating within a single parental granitic magma (e.g., Dahlquist 2002; Donaire et al. 2005), in which case isotope studies can be used to identify these processes. It is noteworthy, therefore, that the Yuhuashan MMEs show higher whole-rock  $\varepsilon_{\text{Nd}}(t)$  values and zircon  $\varepsilon_{\text{Hf}}(t)$  values than the host granite (fig. 12), which therefore rules out the possibility of early crystal segregation for their formation; that is, the MMEs and the host granite must have formed from different magma sources. The MMEs were therefore likely formed by injection of basaltic melt into a magma chamber containing cooler, partially crystalline felsic magma (Waight et al. 2001). This in-

terpretation is supported by the presence of acicular apatite in the MMEs, which is attributed to rapid cooling during mingling of small volumes of hot basalt with a cool granitic melt (Sparks and Marshall 1986).

The elemental and isotopic compositions of the MMEs are distinct from those of the host granite at Yuhuashan (figs. 9, 12, 15), which suggests that chemical diffusion may have been minimized as a result of fast cooling of the subvolcanic granite, which was emplaced at a shallow depth. Furthermore, the higher MgO contents and compatible-element contents of the MMEs also show the chemical characteristics of a mantle-derived magma. Thus, the chemical and isotopic compositions give insight into the composition of the original mantle-derived magma.

Contemporaneous basaltic magmatic rocks have rarely been identified in the GHVB. Jiang et al. (2011) described an Early Cretaceous diabasic dike (ca. 129 Ma) in the middle part of the GHVB that is calc-alkaline, has high  $\text{TiO}_2$  content (fig. 16) and a high  $\varepsilon_{\text{Nd}}(t)$  value (+0.9; fig. 15) and has been suggested to be derived from the asthenospheric mantle wedge. However, the MMEs hosted in the Yuhuashan Complex have negative whole-rock  $\varepsilon_{\text{Nd}}(t)$  and zircon  $\varepsilon_{\text{Hf}}(t)$  values, implying that the MMEs did not form directly from partial melting of the asthenospheric mantle (fig. 15). This hypothesis is further supported by the low  $\text{TiO}_2$  contents in these MMEs (fig. 16). The Yuhuashan MMEs have relatively high  $\text{K}_2\text{O}$  contents and show shoshonitic affinities, and it has been proposed that most

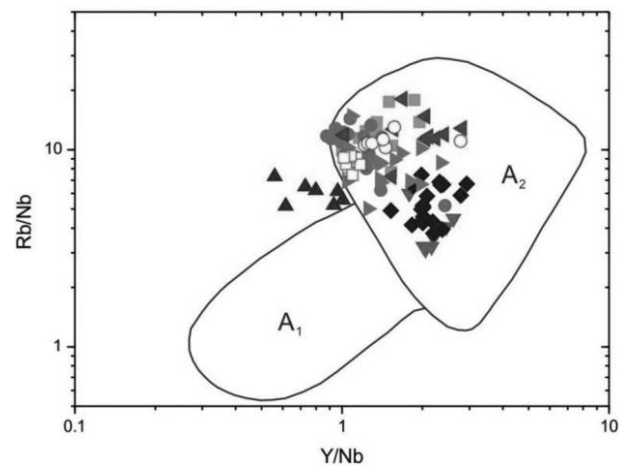


**Figure 14.** Y/Nb-versus-Rb/Nb classification diagram of Eby et al. (1992) for the Early Cretaceous volcanic rocks and granites in the Gan-Hang Belt. Symbols and data sources are as in figure 13. A color version of this figure is available online.

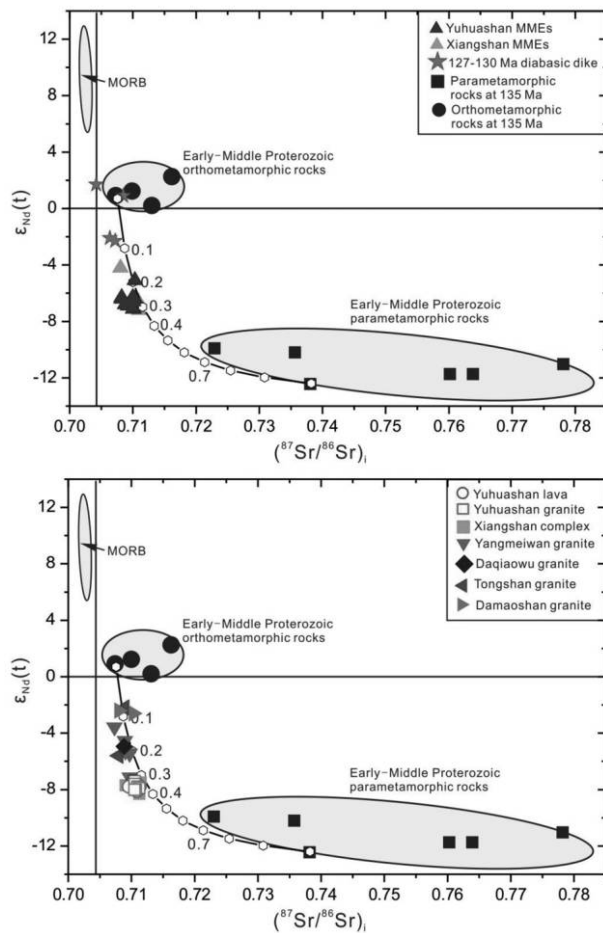


**Figure 15.** Plots of  $\epsilon_{\text{Nd}}(t)$  versus initial  $^{87}\text{Sr}/^{86}\text{Sr}$  ( $(^{87}\text{Sr}/^{86}\text{Sr})_i$ ) for the Yuhuashan Complex and its mafic microgranular enclaves (MMEs), the MMEs in the Xiangshan Complex, and a ca. 129 Ma diabasic dike in the Gan-Hang Belt. Data sources: this study for the Yuhuashan Complex and its MMEs; Jiang et al. (2005) for the Xiangshan Complex and its MMEs; Jiang et al. (2011) and Xia et al. (2016) for the diabasic dike; Yang et al. (2012) for the Yangmeiwan and the Daqiaowu granites; Jiang et al. (2011) for the Tongshan and Damaoshan granites; and table 8 of Jiang et al. (2005) for the parametamorphic and orthometamorphic rocks in the studied area. The orthometamorphic rock sample Fm-13 ([Sr] = 134 ppm,  $^{87}\text{Sr}/^{86}\text{Sr}$  = 0.70757; [Nd] = 11.8 ppm,  $\epsilon_{\text{Nd}}(t)$  = +0.7) and the parametamorphic rock sample Fm-18 ([Sr] = 47 ppm,  $^{87}\text{Sr}/^{86}\text{Sr}$  = 0.73824; [Nd] = 39.1 ppm,  $\epsilon_{\text{Nd}}(t)$  = -12.4; table 8 of Jiang et al. 2005) were adopted as end members to model the mixing line. MORB = mid-ocean ridge basalt. A color version of this figure is available online.

shoshonitic rocks are derived from partial melting of enriched continental lithospheric mantle that has been modified by subducted slab-derived fluids or melts (e.g., Wyllie and Sekine 1982; Peccerillo 1990; Foley and Peccerillo 1992; Turner et al. 1996;

Ersoy et al. 2010, 2013). The negative Nb-Ta anomaly of the MMEs is typical of an arc-type signature (fig. 10), also suggesting that the sources have been metasomatized by previous subduction-related fluids or melt. The Yuhuashan MMEs show high Rb/Sr (0.24–0.72) and low Ba/Rb (2.59–7.82), which strongly suggest that the enclave magma formed through melting of a phlogopite-bearing mantle source (Furman and Graham 1999). Indeed, the Yuhuashan MMEs show a general enrichment in large-ion lithophile elements (e.g., K, Rb, Cs, Th, and U) of the type observed in phlogopite-bearing harzburgite xenoliths from Batan, Luzon arc (Maury et al. 1992).

**Tectonic Setting of the GHVB during the Early Cretaceous.** It has long been recognized that A-type magmas are formed in a variety of extensional regimes, from continental arc or backarc extension to postcollisional extension and within-plate extension (e.g., Eby 1992; Whalen et al. 1996). Eby (1992) suggested that the A<sub>1</sub> group is restricted to hotspots, plumes, and continental rift zones, whereas the A<sub>2</sub> group is more closely associated with postcollisional extension and/or the waning stages of arc magmatism. All of the Early Cretaceous A-type volcanic-intrusive complexes along the GHVB be-

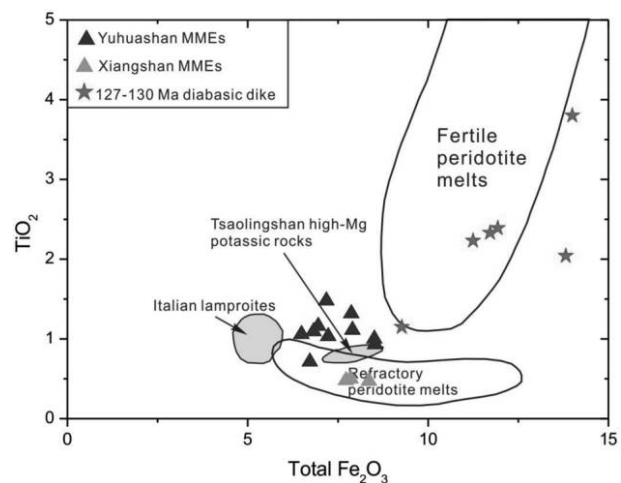


**Figure 16.** Plot of  $\text{TiO}_2$  versus total  $\text{Fe}_2\text{O}_3$  (wt%) for the Yuhuashan mafic microgranular enclaves (MMEs), the Xiangshan MMEs, and the diabasic dike, comparing with fields for some high-Mg potassic rocks and experimental peridotite melts. Data sources: this study for the Yuhuashan MMEs; Jiang et al. (2005) for the Xiangshan MMEs; Jiang et al. (2011) and Xia et al. (2016) for the ca. 129 Ma diabasic dike; Chung et al. (2001) for the Tsaoingshan high-Mg potassic rocks; Peccerillo (1999) for the Italian lamproites; and Falloon et al. (1988) for the experimental melts. A color version of this figure is available online.

long to the  $A_2$  subtype (fig. 14); thus, an origin related to a hotspot, plume, or continental rift zone is unlikely. As shown in the figure 17, samples from the Yuhuashan Complex plot in the field of volcanic arc granites, but most of the later granites (e.g., the Tongshan and the Damaoshan granites) plot in the field of within-plate granites (fig. 17).

Shoshonitic rocks typically occur in destructive plate margin settings as the arc matures (Morrison 1980), with these and other potassic rocks occurring in extensional environments such as postcollisional and continental rift tectonic settings (e.g., Müller et al. 1992; Rogers 1992; Turner et al. 1996; Eklund

et al. 1998; Ersoy et al. 2010, 2013). The Yuhuashan MMEs plot in the continental arc field in the discrimination diagram (fig. 17). The apparent change from the melting of the lithospheric mantle at ca. 135 Ma to the melting of the asthenospheric mantle at ca. 129 Ma also indicates that continental extension gradually intensified over this interval and that the lithospheric mantle progressively thinned. A similar situation has been observed for the volcanism in the Aegean region in Turkey, where the ocean-island basalt–like Kula volcanic rocks were emplaced in the Quaternary, after the main-stage Eocene–Miocene potassic volcanism (Ersoy et al. 2013). This change is thought to have been caused by upwelling of asthenospheric mantle as a result of slab rollback or a slab tear (e.g., Ersoy et al. 2013).

Jiang et al. (2011) suggested that an intra-arc rift or a backarc extension developed along the GHVB after the Early Cretaceous (~130 Ma), and Wong et al. (2009) proposed a model of irregular and episodic rollback of the paleo-Pacific plate that led to localized extension in the upper plate. Available ages and geochemical data for the Early Cretaceous A-type granitic rocks along the GHVB (table 1) indicate that intrusive volcanism and, by implication, continental extension commenced as early as ca. 137 Ma at Xiangshan and continued to 122 Ma. The observation of higher  $\epsilon_{Nd}(t)$  values for the later granites (fig. 15) indicates that the mantle-crust interaction in the formation of the A-type granite magma along the GHVB gradually intensified from the early stage to the late stage. The gradual increase in continental extension during this time is consistent with the model of the rollback of a subducted paleo-Pacific-derived plate. Thus, we suggest that a backarc extensional setting is favored to represent the tectonic setting of the GHVB during Early Cretaceous.

We propose an integrated model for the origin of the Yuhuashan Complex and MMEs based on all the observations presented in this article, as shown in figure 18. The lithospheric mantle in the studied area had been metasomatized by subducted slab-derived fluids or melts due to the subduction of a Paleo-Pacific-derived plate before the Early Cretaceous. In the Early Cretaceous (~137–135 Ma), backarc extension and upwelling of the asthenosphere, as a consequence of slab rollback, resulted in partial melting of the enriched lithospheric mantle, generating the potassic basaltic magmas (fig. 18a). Underplating of such high-temperature magmas into the Proterozoic metamorphic crustal region induced partial melting and generated the high-temperature (>800°C) A-type felsic magmas. The felsic magma subsequently was erupted to form the

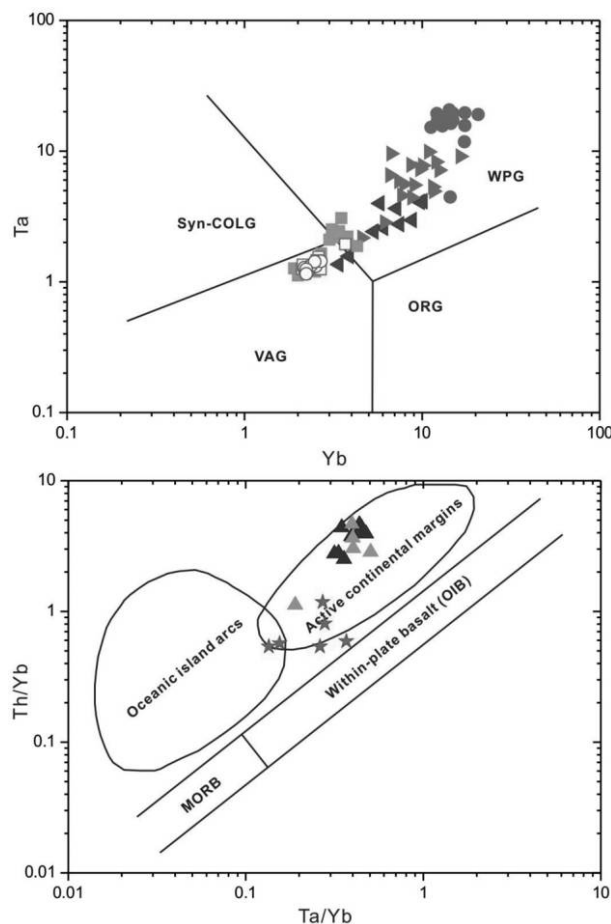


**Figure 17.** *Top*, Yb-versus-Ta diagram (Pearce et al. 1984) for the Yuhuashan Complex, the Damaoshan granite, the Tongshan granite, and the Baijuhuajian granite. ORG = ocean ridge granite; syn-COLG = syncollision granite; VAG = volcanic arc granite; WPG = within-plate granite. *Bottom*, Ta/Yb-versus-Th/Yb diagram (Pearce 1982) for the Yuhuashan mafic microgranular enclaves (MMEs), the Xiangshan MMEs, and the diabase dikes. OIB = ocean island basalt; MORB = mid-ocean ridge basalt. Symbols and data sources are as in figures 13 and 15. A color version of this figure is available online.

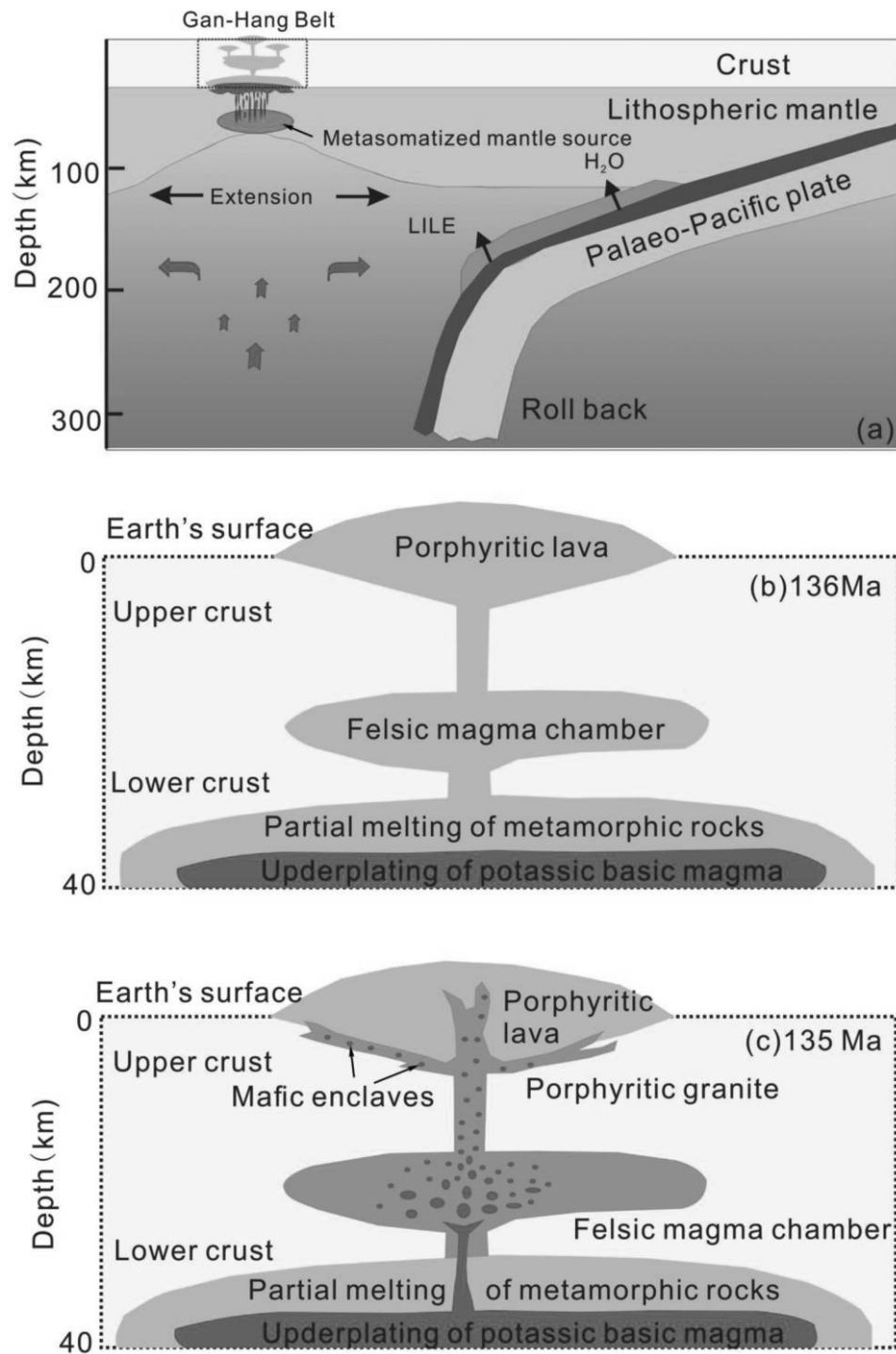


**Figure 18.** Cartoons showing the integrated genesis model for the Yuhuashan Complex and its mafic microgranular enclaves. LILE = large-ion lithophile elements. See the text for the details. A color version of this figure is available online.

Yuhuashan lava (fig. 18b). Meanwhile, the mafic magma was injected into the felsic magma chamber to form discrete magma blobs (e.g., Waight et al. 2001). Then, the felsic magma containing mafic

magma blobs ascended along the volcanic vent or ring fractures to form the Yuhuashan porphyritic granite and MMEs (fig. 18c). With ongoing rollback of the subducted slab (130–122 Ma), the partial

melting of upwelling asthenospheric mantle would generate the diabasic dikes (e.g., Tongshan and Miaohou-Shanhou). Injecting and mixing of more mantle magma into the felsic magma would result in higher  $\epsilon_{Nd}(t)$  values for these later A-type granites (e.g., Tongshan, Damaoshan, Baijuhajian, Miaohou-Shanhou, and Furongshan).

**Implication for Exploration of U Mining.** The GHVB is the most important volcanic-rock-hosted uranium mine belt in China. Several large-scale uranium orefields (e.g., Xiangshan, Shengyuan, Daqiaowu, and Dazhou) occur in these Early Cretaceous volcanic basins. U orebodies occur as veins and are hosted by volcanic rocks and granite porphyry. The U mineralization ages are younger than the formation ages of these hosting volcanic complexes (Hu et al. 2008). According to the classification of U ore deposits by Cuney (2009), these U ore deposits in the GHVB belong to the hydrothermal vein type. Most researchers have suggested these volcanic rocks as U sources for mineralization (e.g., Hu et al. 2008). Thus, discrimination of U-bearing and barren rocks is important for exploring more U deposits in this belt.

The Xiangshan Complex, which lies to the southeast of the Yuhushan Complex (fig. 1), hosts the largest uranium orefield in South China, with U reserves of above 20,000 tons. Until now, no economic uranium mineralization has been found in the Yuhuashan Complex. The U contents of the Yuhuashan Complex (3–5 ppm) are similar to those of the Xiangshan Complex (Yang et al. 2011). According to this study, the formation age, petrography, geochemistry, and isotopic compositions of the Yuhuashan Complex are also comparable to those of the Xiangshan Complex. Thus, there are no differences between the Yuhuashan and the Xiangshan Complexes in terms of their being U sources for mineralization. Evaluation of the Yuhuashan Complex for potential U mineralization

must consider other ore-forming factors (e.g., fluids, faults, and reduced agents).

### Conclusions

1. The LA-ICP-MS zircon U-Pb geochronology indicates that the Yuhuashan volcanic-intrusive rocks formed during the Early Cretaceous (ca. 136–135 Ma).
2. The Yuhuashan Complex shows A-type geochemical characteristics and can be further classified into the A<sub>2</sub> subtype. It was generated largely by partial melting of Proterozoic basement rocks (including parametamorphic and orthometamorphic rocks).
3. Mafic microgranular enclaves in the Yuhushan Complex originated from magma mingling, and the primary magmas were derived from the enriched lithospheric mantle, which had been metasomatized by previous subduction-related fluids or melt.
4. The Early Cretaceous A<sub>2</sub>-type granitic rocks, with ages of 137–122 Ma, occurred along the GHVB, indicating an important extensional event. A backarc extensional setting, related to the rollback of a subducted paleo-Pacific-derived plate, is favored to explain the petrogenesis of the Yuhushan Complex and its MMEs.

### ACKNOWLEDGMENTS

This work is supported by the National Key Research and Development Program of China (2017YFC0601404) and the National Natural Science Foundation of China (projects 41273038 and 91755208). We are grateful to editor D. B. Rowley, reviewer M. R. Palmer, and an anonymous reviewer for helpful comments that clearly improved this article.

### REFERENCES CITED

- Allen, C. M. 1991. Local equilibrium of mafic enclaves and granitoids of the Turtle pluton, southeast California: mineral, chemical, and isotopic evidence. *Am. Mineral.* 76:574–588.
- Andersen, T. 2002. Correction of common Pb in U-Pb analyses that do not report <sup>204</sup>Pb. *Chem. Geol.* 192:59–79.
- Barbarin, B. 2005. Mafic magmatic enclaves and mafic rocks associated with some granitoids of the central Sierra Nevada batholith, California: nature, origin, and relations with the hosts. *Lithos* 80(1–4):155–177.
- Blichert-Toft, J., and Albarède, F. 1997. The Lu-Hf isotope geochemistry of chondrites and the evolution of the mantle-crust system. *Earth Planet. Sci. Lett.* 148(1–2):243–258.
- Bonin, B. 2007. A-type granites and related rocks: evolution of a concept, problems and prospects. *Lithos* 97(1–2):1–29.
- Boynton, W. L. 1984. Geochemistry of the rare earth elements: meteorite studies. In Henderson, P., ed. *Rare earth element geochemistry*. Amsterdam, Elsevier, p. 63–114.
- Chappell, B. W.; White, A. J. R.; and Wyborn, D. 1987. The importance of residual source material (restite) in granite petrogenesis. *J. Petrol.* 28(6):1111–1138.

- Charvet, J. 2013. The Neoproterozoic–Early Paleozoic tectonic evolution of the South China Block: an overview. *J. Asian Earth Sci.* 74:198–209.
- Charvet, J.; Lapiere, H.; and Yu, Y. 1994. Geodynamic significance of the Mesozoic volcanism of southeastern China. *J. Southeast Asian Earth Sci.* 9(4):387–396.
- Chen, J., and Jahn, B.-M. 1998. Crustal evolution of southeastern China: Nd and Sr isotopic evidence. *Tectonophysics* 284(1–2):101–133.
- Chung, S.-L.; Wang, K.-L.; Crawford, A. J.; Kamenetsky, V. S.; Chen, C.-H.; Lan, C.-Y.; and Chen, C.-H. 2001. High-Mg potassic rocks from Taiwan: implications for the genesis of orogenic potassic lavas. *Lithos* 59(4):153–170.
- Cuney, M. 2009. The extreme diversity of uranium deposits. *Miner. Depos.* 44(1):3–9.
- Dahlquist, J. A. 2002. Mafic microgranular enclaves: early segregation from metaluminous magma (Sierra de Chepes), Pampean Ranges, NW Argentina. *J. S. Am. Earth Sci.* 15(6):643–655.
- Didier, J., and Barbarin, B., eds. 1991. Enclaves and granite petrology. *Developments in Petrology*, no. 13. Amsterdam, Elsevier. 625 p.
- Donaire, T.; Pascual, E.; Pin, C.; and Duthou, J.-L. 2005. Microgranular enclaves as evidence of rapid cooling in granitoid rocks: the case of the Los Pedroches granodiorite, Iberian Massif, Spain. *Contrib. Mineral. Petrol.* 149(3):247–265.
- Eby, G. N. 1992. Chemical subdivision of the A-type granitoids: petrogenetic and tectonic implications. *Geology* 20:641–644.
- Eklund, O.; Konopelko, D.; Rutanen, H.; Fröjdö, S.; and Shebanov, A. D. 1998. 1.8 Ga Svecofennian post-collisional shoshonitic magmatism in the Fennoscandian shield. *Lithos* 45(1–4):87–108.
- Ersoy, E. Y.; Helvacı, C.; and Palmer, M. R. 2010. Mantle source characteristics and melting models for the early-middle Miocene mafic volcanism in western Anatolia: implications for enrichment processes of mantle lithosphere and origin of K-rich volcanism in post-collisional settings. *J. Volcanol. Geotherm. Res.* 198:112–128.
- Ersoy, E. Y., and Palmer, M. R. 2013. Eocene–Quaternary magmatic activity in the Aegean: implications for mantle metasomatism and magma genesis in an evolving orogeny. *Lithos* 180–181:5–24.
- Fallon, T. J.; Green, D. H.; Hatton, C. J.; and Harris, K. L. 1988. Anhydrous partial melting of a fertile and depleted peridotite from 2 to 30 kb and application to basalt petrogenesis. *J. Petrol.* 29(6):1257–1282.
- Foley, S., and Peccerillo, A. 1992. Potassic and ultrapotassic magmas and their origin. *Lithos* 28(3–6):181–185.
- Furman, T., and Graham, D. 1999. Erosion of lithospheric mantle beneath the East African Rift system: geochemical evidence from the Kivu volcanic province. *Lithos* 48(1–4):237–262.
- Gao, J. F.; Lu, J. J.; Lai, M. Y.; Lin, Y. P.; and Pu, W. 2003. Analysis of trace elements in rock samples using HR-ICP-MS. *J. Nanjing Univ. (Nat. Sci.)* 39:844–850 (in Chinese with English abstract).
- Gilder, S. A.; Gill, J.; Coe, R. S.; Zhao, X. X.; Liu, Z. W.; and Wang, G. X. 1996. Isotopic and paleomagnetic constraints on the Mesozoic tectonic evolution of South China. *J. Geophys. Res.* 101(B7):16,137–16,154.
- Gilder, S. A.; Keller, G. R.; Luo, M.; and Goodell, P. C. 1991. Eastern Asia and the western Pacific: timing and spatial distribution of rifting in China. *Tectonophysics* 197(2–4):225–243.
- Hoskin, P. W. O., and Schaltegger, U. 2003. The composition of zircon and igneous and metamorphic petrogenesis. *In* Hancher, J. M., and Hoskin, P. W. O., eds. *Zircon. Rev. Mineral. Geochem.* 53:27–62.
- Hu, G. R., and Zhang, B. T. 1998. Neodymium isotope composition and source materials of the metabasement in central Jiangxi Province. *Acta Petrol. Mineral.* 17(1):35–40 (in Chinese with English abstract).
- Hu, R. Z.; Bi, X. W.; Peng, J. T.; Liu, S.; Zhong, H.; Zhao, J. H.; and Jiang, G. H. 2008. Uranium metallogenesis in South China and its relationship to crustal extension during the Cretaceous to Tertiary. *Econ. Geol.* 103:583–598.
- Jacobsen, S. B., and Wasserburg, G. J. 1980. Sm–Nd isotopic evolution of chondrites. *Earth Planet. Sci. Lett.* 50:139–155.
- Jahn, B.-M., and Condie, K. C. 1995. Evolution of the Kaapvaal Craton as viewed from geochemical and Sm–Nd isotopic analyses of intracratonic pelites. *Geochim. Cosmochim. Acta* 59(11):2239–2258.
- Jahn, B. M.; Zhou, X. H.; and Li, J. L. 1990. Formation and tectonic evolution of southeastern China and Taiwan: isotopic and geochemical constraints. *Tectonophysics* 183(1–4):145–160.
- Jiang, Y. H.; Ling, H. F.; Jiang, S. Y.; Fan, H. H.; Shen, W. Z.; and Ni, P. 2005. Petrogenesis of a Late Jurassic peraluminous volcanic complex and its high-Mg, potassic, quenched enclaves at Xiangshan, Southeast China. *J. Petrol.* 46(6):1121–1154.
- Jiang, Y. H.; Zhao, P.; Zhou, Q.; Liao, S. Y.; and Jin, G. D. 2011. Petrogenesis and tectonic implications of Early Cretaceous S- and A-type granites in the northwest of the Gan-Hang rift, SE China. *Lithos* 121(1–4):55–73.
- Jung, S., and Pfänder, J. A. 2007. Source composition and melting temperatures of orogenic granitoids: constraints from CaO/Na<sub>2</sub>O, Al<sub>2</sub>O<sub>3</sub>/TiO<sub>2</sub> and accessory mineral saturation thermometry. *Eur. J. Mineral.* 19(6):859–870.
- Kelemen, P. B.; Hanghoj, K.; and Greene, A. R. 2003. One view of the geochemistry of subduction-related magmatic arcs, with an emphasis on primitive andesite and lower crust. *In* Rudnick, R. L., ed. *The crust. Treatise on geochemistry* 3:593–660.
- King, P. L.; Chappell, B. W.; Allen, C. M.; and White, A. J. R. 2001. Are A-type granites the high-temperature felsic granites? evidence from fractionated granites of the Wangrah Suite. *Aust. J. Earth Sci.* 48:501–514.

- Lapierre, H.; Jahn, B. M.; Charvet, J.; and Yu, Y. W. 1997. Mesozoic felsic arc magmatism and continental olivine tholeiites in Zhejiang Province and their relationship with the tectonic activity in southeastern China. *Tectonophysics* 274(4):321–338.
- Le Bas, M. J.; Le Maitre, R. W.; Streckeisen, A.; and Zanettin, B. 1986. A chemical classification of volcanic rocks based on the total alkali-silica diagram. *J. Petrol.* 27(3):745–750.
- Li, J.; Zhang, Y.; Dong, S.; and Johnston, S. T. 2014. Cretaceous tectonic evolution of South China: a preliminary synthesis. *Earth-Sci. Rev.* 134:98–136.
- Li, X. H.; Li, W. X.; Li, Z. X.; Lo, C. H.; Wang, J.; Ye, M.-F.; and Yang, Y.-H. 2009. Amalgamation between the Yangtze and Cathaysia Blocks in South China: constraints from SHRIMP U-Pb zircon ages, geochemistry and Nd-Hf isotopes of the Shuangxiwu volcanic rocks. *Precambrian Res.* 174(1–2):117–128.
- Li, Z. X., and Li, X. H. 2007. Formation of the 1300-km-wide intracontinental orogen and postorogenic magmatic province in Mesozoic South China: a flat-slab subduction model. *Geology* 35(2):179–182.
- Liu, L.; Xu, X.; and Xia, Y. 2014. Cretaceous Pacific plate movement beneath SE China: evidence from episodic volcanism and related intrusions. *Tectonophysics* 614:170–184.
- Liu, Y. S.; Gao, S.; Hu, Z. C.; Gao, C. G.; Zong, K. Q.; and Wang, D. B. 2010a. Continental and oceanic crust recycling-induced melt-peridotite interactions in the Trans-North China Orogen: U-Pb dating, Hf isotopes and trace elements in zircons from mantle xenoliths. *J. Petrol.* 51(1–2):537–571.
- Liu, Y. S.; Hu, Z. C.; Zong, K. Q.; Gao, C. G.; Gao, S.; Xu, J.; and Chen, H. H. 2010b. Reappraisal and refinement of zircon U-Pb isotope and trace element analyses by LA-ICP-MS. *Chin. Sci. Bull.* 55:1535–1546.
- Loiselle, M. C., and Wones, D. R. 1979. Characteristics and origin of anorogenic granites. In *Annual Meetings of the Geological Society of America and Associated Societies* (San Diego, CA, 1979), Abstracts, 11:468.
- Lugmair, G. W., and Marti, K. 1978. Lunar initial  $^{143}\text{Nd}/^{144}\text{Nd}$ : differential evolution of the lunar crust and mantle. *Earth Planet. Sci. Lett.* 39:349–357.
- Maas, R.; Nicholls, I. A.; and Legg, C. 1997. Igneous and metamorphic enclaves in the S-type Deddick granodiorite, Lachlan Fold Belt, SE Australia: petrographic, geochemical and Nd-Sr isotopic evidence for crustal melting and magma mixing. *J. Petrol.* 38(7):815–841.
- Mao, J. W.; Chen, M. H.; Yuan, X. D.; and Guo, C. L. 2011. Geological characteristics of the Qin-Hang (or Shi-Hang) metallogenic belt in South China and spatial-temporal distribution regularity of mineral deposits. *Acta Geol. Sin.* 85(5):636–658 (in Chinese with English abstract).
- Maury, R. C.; Defant, M. J.; and Joron, J.-L. 1992. Metasomatism of the sub-arc mantle inferred from trace elements in Philippine xenoliths. *Nature* 360(6405):661–663.
- Miller, C. F.; McDowell, S. M.; and Mapes, R. W. 2003. Hot and cold granites? implications of zircon saturation temperatures and preservation of inheritance. *Geology* 31(6):529–532.
- Morrison, G. W. 1980. Characteristics and tectonic setting of the shoshonite rock association. *Lithos* 13:97–108.
- Müller, D.; Rock, N. M. S.; and Groves, D. I. 1992. Geochemical discrimination between shoshonitic and potassic volcanic rocks in different tectonic settings: a pilot study. *Mineral. Petrol.* 46(4):259–289.
- Nowell, G. M.; Kempton, P. D.; Noble, S. R.; Fitton, J. G.; Saunders, A. D.; Mahoney, J. J.; and Taylor, R. N. 1998. High precision Hf isotope measurements of MORB and OIB by thermal ionisation mass spectrometry: insights into the depleted mantle. *Chem. Geol.* 149(3–4):211–233.
- Pearce, J. A. 1982. Trace element characteristics of lava from destructive plate boundaries. In *Thorps, R. S., ed. Andesites*. Chichester, Wiley, p. 525–548.
- Pearce, J. A.; Harris, N. B. W.; and Tindle, A. G. 1984. Trace element discrimination diagrams for the tectonic interpretation of granitic rocks. *J. Petrol.* 25(4):956–983.
- Peccerillo, A. 1990. On the origin of the Italian potassic magmas—comments. *Chem. Geol.* 85(1–2):183–191.
- . 1999. Multiple mantle metasomatism in central-southern Italy: geochemical effects, timing and geodynamic implications. *Geology* 27(4):315–318.
- Perugini, D.; Poli, G.; Christofides, G.; and Eleftheriadis, G. 2003. Magma mixing in the Sithonia Plutonic Complex, Greece: evidence from mafic microgranular enclaves. *Mineral. Petrol.* 78(3):173–200.
- Pu, W.; Gao, J. F.; Zhao, K. D.; Ling, H. F.; and Jiang, S. Y. 2005. Separation method of Rb-Sr, Sm-Nd using DCTA and HIBA. *J. Nanjing Univ. (Nat. Sci.)* 41:445–450 (in Chinese with English abstract).
- Qiu, Y. M.; Gao, S.; McNaughton, N. J.; Groves, D. I.; and Ling, W. L. 2000. First evidence of >3.2 Ga continental crust in the Yangtze craton of south China and its implications for Archean crustal evolution and Phanerozoic tectonics. *Geology* 28(1):11–14.
- Rogers, N. W. 1992. Potassic magmatism as a key to trace-element enrichment processes in the upper mantle. *J. Volcanol. Geotherm. Res.* 50(1–2):85–99.
- Shu, X.; Yang, S. Y.; Jiang, S. Y.; and Ye, M. 2017. Petrogenesis and geodynamic setting of Early Cretaceous felsic rocks in the Gan-Hang Belt, Southeast China: constraints from geochronology and geochemistry of the tuffs and trachyandesitic rocks in Shengyuan volcanic basin. *Lithos* 284–285:691–708.
- Sláma, J.; Košler, J.; Condon, D. J.; Crowley, J. L.; Gerdes, A.; Hanchar, J. M.; Horstwood, M. S. A.; et al. 2008. Plešovice zircon—a new natural reference material for U-Pb and Hf isotopic microanalysis. *Chem. Geol.* 249(1–2):1–35.

- Sparks, R. S. J., and Marshall, L. 1986. Thermal and mechanical constraints on mixing between mafic and silicic magmas. *J. Volcanol. Geotherm. Res.* 29:99–124.
- Sun, S. S., and McDonough, W. F. 1989. Chemical and isotopic systematics of oceanic basalt: implications for mantle composition and processes. *In* Saunders, A. D., and Norry, M. J., eds. *Magmatism in the ocean basins*. Geol. Soc. Lond. Spec. Publ. 42:528–548.
- Sun, W. D.; Ding, X.; Hu, Y. H.; and Li, X. H. 2007. The golden transformation of the Cretaceous plate subduction in the west Pacific. *Earth Planet. Sci. Lett.* 262(3–4):533–542.
- Turner, S.; Arnaud, N.; Liu, J.; Rogers, N.; Hawkesworth, C.; Harris, N.; Kelley, S.; van Calsteren, P.; and Deng, W. 1996. Post-collision, shoshonitic volcanism on the Tibetan Plateau: implications for convective thinning of the lithosphere and the source of ocean island basalts. *J. Petrol.* 37(1):45–71.
- Vernon, R. H. 1984. Microgranitoid enclaves in granites: globules of hybrid magma quenched in a plutonic environment. *Nature* 309:438–439.
- Vernon, R. H.; Etheridge, M. A.; and Wall, V. J. 1988. Shape and microstructure of microgranitoid enclaves: indicators of magma mingling and flow. *Lithos* 22(1):1–11.
- Waight, T. E.; Maas, R.; and Nicholls, I. A. 2001. Geochemical investigations of microgranitoid enclaves in the S-type Cowra Granodiorite, Lachlan Fold Belt, SE Australia. *Lithos* 56(2–3):165–186.
- Wang, D. Z., and Zhou, J. C. 2005. New progress in studying the large igneous provinces. *Geol. J. China Univ.* 11(1):1–8 (in Chinese with English abstract).
- Wang, H. Z.; Chen, P. R.; Sun, L. Q.; Ling, H. F.; Zhao, Y. D.; and Lan, H. F. 2015. Magma mixing and crust-mantle interaction in Southeast China during the Early Cretaceous: evidence from the Furongshan granite porphyry and mafic microgranular enclaves. *J. Asian Earth Sci.* 111:72–87.
- Watson, E. B., and Harrison, T. M. 1983. Zircon saturation revisited: temperature and composition effects in a variety of crustal magma types. *Earth Planet. Sci. Lett.* 64:295–304.
- Whalen, J. B.; Currie, K. L.; and Chappell, B. W. 1987. A-type granites: geochemical characteristics, discrimination and petrogenesis. *Contrib. Mineral. Petrol.* 95(4):407–419.
- Whalen, J. B.; Jenner, G. A.; Longstaffe, F. J.; Robert, F.; and Gariépy, C. 1996. Geochemical and isotopic (O, Nd, Pb and Sr) constraints on A-type granite petrogenesis based on the Topsails Igneous Suite, Newfoundland Appalachians. *J. Petrol.* 37(6):1463–1489.
- White, A. J. R.; Chappell, B. W.; and Wyborn, D. 1999. Application of the restite model to the Deddick granodiorite and its enclaves—a reinterpretation of the observations and data of Maas *et al.* (1997). *J. Petrol.* 40(3):413–421.
- Wiedenbeck, M.; Hanchar, J. M.; Peck, W. H.; Sylvester, P.; Valley, J.; Whitehouse, M.; Kronz, A.; et al. 2004. Further characterisation of the 91500 zircon crystal. *Geostand. Geoanal. Res.* 28(1):9–39.
- Williams, I. S. 1992. Some observations on the use of zircon U-Pb geochronology in the study of granitic rocks. *Earth Environ. Sci. Trans. R. Soc. Edinb.* 83(1–2):447–458.
- Wong, J.; Sun, M.; Xing, G.; Li, X.-H.; Zhao, G.; Wong, K.; Yuan, C.; Xia, X.; Li, L.; and Wu, F. 2009. Geochemical and zircon U-Pb and Hf isotopic study of the Baijuhuajian metaluminous A-type granite: extension at 125–100 Ma and its tectonic significance for South China. *Lithos* 112(3–4):289–305.
- Wu, F. Y.; Yang, Y. H.; Xie, L. W.; Yang, J. H.; and Xu, P. 2006. Hf isotopic compositions of the standard zircons and baddeleyites used in U-Pb geochronology. *Chem. Geol.* 234(1–2):105–126.
- Wu, Y. B., and Zheng, Y. F. 2004. Genesis of zircon and its constraints on interpretation of U-Pb age. *Chin. Sci. Bull.* 49(15):1554–1569.
- Wyllie, P., and Sekine, T. 1982. The formation of mantle phlogopite in subduction zone hybridization. *Contrib. Mineral. Petrol.* 79(4):375–380.
- Xia, Y.; Xu, X.; and Liu, L. 2016. Transition from adakitic to bimodal magmatism induced by the paleo-Pacific plate subduction and slab rollback beneath SE China: evidence from petrogenesis and tectonic setting of the dike swarms. *Lithos* 244:182–204.
- Xu, X.; O'Reilly, S. Y.; Griffin, W. L.; Wang, X.; Pearson, N. J.; and He, Z. 2007. The crust of Cathaysia: age, assembly and reworking of two terranes. *Precambrian Res.* 158(1–2):51–78.
- Yang, J. H.; Wu, F. Y.; Wilde, S. A.; Xie, L. W.; Yang, Y. H.; and Liu, X. M. 2007. Tracing magma mixing in granite genesis: in-situ U-Pb dating and Hf isotope analysis of zircons. *Contrib. Mineral. Petrol.* 153(2):177–190.
- Yang, S. Y.; Jiang, S. Y.; Jiang, Y. H.; Zhao, K. D.; and Fan, H. H. 2011. Geochemical, zircon U-Pb dating and Sr-Nd-Hf isotopic constraints on the age and petrogenesis of an Early Cretaceous volcanic-intrusive complex at Xiangshan, Southeast China. *Mineral. Petrol.* 101(1–2):21–48.
- Yang, S. Y.; Jiang, S. Y.; Zhao, K. D.; and Jiang, Y. H. 2013. Petrogenesis and tectonic significance of Early Cretaceous high-Zr rhyolite in the Dazhou uranium district, Gan-Hang Belt, Southeast China. *J. Asian Earth Sci.* 74:303–315.
- Yang, S. Y.; Jiang, S. Y.; Zhao, K. D.; Jiang, Y. H.; Ling, H. F.; and Luo, L. 2012. Geochronology, geochemistry and tectonic significance of two Early Cretaceous A-type granites in the Gan-Hang Belt, Southeast China. *Lithos* 150:155–170.
- Zhao, K. D.; Jiang, S. Y.; Yang, S. Y.; Dai, B. Z.; and Lu, J. J. 2012. Mineral chemistry, trace elements and Sr-Nd-Hf isotope geochemistry and petrogenesis of Cailing and Furong granites and mafic enclaves from the Qitianling batholith in the Shi-Hang zone, South China. *Gondwana Res.* 22(1):310–324.
- Zhao, K. D.; Jiang, S. Y.; Zhu, J. C.; Li, L.; Dai, B. Z.; Jiang, Y. H.; and Ling, H. F. 2010. Hf isotopic com-

- position of zircons from the Huashan-Guposhan intrusive complex and their mafic enclaves in northeastern Guangxi: implication for petrogenesis. *Chin. Sci. Bull.* 55(6):509–519.
- Zhou, J.; Jiang, Y. H.; Xing, G. F.; Zeng, Y.; and Ge, W. Y. 2013. Geochronology and petrogenesis of Cretaceous A-type granites from the NE Jiangnan orogen, SE China. *Int. Geol. Rev.* 55(11):1359–1383.
- Zhou, X. M., and Li, W. X. 2000. Origin of late Mesozoic igneous rocks in southeastern China: implications for lithosphere subduction and underplating of mafic magmas. *Tectonophysics* 326(3–4):269–287.
- Zhou, X. M.; Sun, T.; Shen, W. Z.; Shu, L. S.; and Niu, Y. L. 2006. Petrogenesis of Mesozoic granitoids and volcanic rocks in South China: a response to tectonic evolution. *Episodes* 29(1); 26–33.